Failure Analysis of Sapphire Refractive Secondary Concentrators

Jonathan A. Salem
Glenn Research Center, Cleveland, Ohio

George D. Quinn
National Institute of Standards and Testing, Gaithersburg, Maryland

NASA STI Program . . . in Profile

Since its founding, NASA has been dedicated to the advancement of aeronautics and space science. The NASA Scientific and Technical Information (STI) program plays a key part in helping NASA maintain this important role.

The NASA STI Program operates under the auspices of the Agency Chief Information Officer. It collects, organizes, provides for archiving, and disseminates NASA's STI. The NASA STI program provides access to the NASA Aeronautics and Space Database and its public interface, the NASA Technical Reports Server, thus providing one of the largest collections of aeronautical and space science STI in the world. Results are published in both non-NASA channels and by NASA in the NASA STI Report Series, which includes the following report types:

- TECHNICAL PUBLICATION. Reports of completed research or a major significant phase of research that present the results of NASA programs and include extensive data or theoretical analysis. Includes compilations of significant scientific and technical data and information deemed to be of continuing reference value. NASA counterpart of peer-reviewed formal professional papers but has less stringent limitations on manuscript length and extent of graphic presentations.

- TECHNICAL MEMORANDUM. Scientific and technical findings that are preliminary or of specialized interest, e.g., quick release reports, working papers, and bibliographies that contain minimal annotation. Does not contain extensive analysis.

- CONTRACTOR REPORT. Scientific and technical findings by NASA-sponsored contractors and grantees.

- CONFERENCE PUBLICATION. Collected papers from scientific and technical conferences, symposia, seminars, or other meetings sponsored or cosponsored by NASA.

- SPECIAL PUBLICATION. Scientific, technical, or historical information from NASA programs, projects, and missions, often concerned with subjects having substantial public interest.

- TECHNICAL TRANSLATION. English-language translations of foreign scientific and technical material pertinent to NASA's mission.

Specialized services also include creating custom thesauri, building customized databases, organizing and publishing research results.

For more information about the NASA STI program, see the following:

- Access the NASA STI program home page at *http://www.sti.nasa.gov*

- E-mail your question via the Internet to *help@ sti.nasa.gov*

- Fax your question to the NASA STI Help Desk at 443–757–5803

- Telephone the NASA STI Help Desk at 443–757–5802

- Write to:
  NASA Center for AeroSpace Information (CASI)
  7115 Standard Drive
  Hanover, MD 21076–1320

Failure Analysis of Sapphire Refractive Secondary Concentrators

Jonathan A. Salem
Glenn Research Center, Cleveland, Ohio

George D. Quinn
National Institute of Standards and Testing, Gaithersburg, Maryland

National Aeronautics and
Space Administration

Glenn Research Center
Cleveland, Ohio 44135

December 2009

Acknowledgments

The authors thank Charlie Castle and Wayne Wong or many useful discussions,
Rick Rogers for x-ray diffraction, and Terry McCue for electron microscopy.

Failure Analysis of Sapphire Refractive Secondary Concentrators

Jonathan A. Salem
National Aeronautics and Space Administration
Glenn Research Center
Cleveland, Ohio 44135

George D. Quinn
National Institute of Standards and Testing
Gaithersburg, Maryland 20899

Abstract

Failure analysis was performed on two sapphire, refractive secondary concentrators(RSC) that failed during elevated temperature testing. Both concentrators failed from machining/handling damage on the lens face. The first concentrator, which failed during testing to 1300 °C, exhibited a large r-plane twin extending from the lens through much of the cone. The second concentrator, which was an attempt to reduce temperature gradients and failed during testing to 649 °C, exhibited a few small twins on the lens face. The twins were not located at the origin, but represent another mode of failure that needs to be considered in the design of sapphire components. In order to estimate the fracture stress from fractographic evidence, branching constants were measured on sapphire strength specimens. The fractographic analysis indicated radial tensile stresses of 44 to 65 MPa on the lens faces near the origins. Finite element analysis indicated similar stresses for the first RSC, but lower stresses for the second RSC. Better machining and handling might have prevented the fractures, however, temperature gradients and resultant thermal stresses need to be reduced to prevent twinning.

Introduction

The Sun is a readily available source of thermal energy for space systems if its power can be efficiently harnessed and applied. Refractive secondary concentrators (RSCs) provide higher solar concentration ratios, efficiency, and heat receiver cavity flux tailoring as compared to conventional hollow refractive parabolic concentrator systems (Refs. 1 and 2). The materials considered for RSCs are generally single crystal oxides such as yttria-stabilized zirconia (Y_2O_3-ZrO_2), yttrium-alumina-garnet ($Y_3Al_5O_{12}$ or YAG), magnesium oxide (MgO) or sapphire (Al_2O_3). These materials are very brittle, and the reliability of such RSCs under the thermal shock conditions encountered during space mission sun-shade transitions is of great concern. In addition to thermal shock, an RSC may have large, continuous temperature gradients and associated stresses at elevated temperature depending upon the design. This can lead to slow crack growth and creep in many systems, and in sapphire it can lead to twinning when the stress state involves compression induced shear.

Testing of a single sapphire RSC resulted in catastrophic failure (Ref. 3). A second RSC with a redesigned mounting system to minimize thermal gradients also resulted in failure. This report summarizes the failure analysis and the failure stress estimation for both RSCs, and gives recommendation for future design and testing of RSCs.

Test Conditions Leading to Failure

Both concentrators were machined[1] from Heat Exchange Method grown boules[2] such that the RSC long axis was parallel to the c-axis of the crystal as shown in Figure 1, and the front lens face was normal

---

[1]Computer Optics Inc., Hudson, New Hampshire
[2]Crystal Systems Inc., Salem, Massachusetts

to the *c*-axis. The RSC test assemblies are shown in Figure 2 and details of the test assembly shown in Figure 3.

Testing was performed in NASA Glenn Research Center's Tank 6 under vacuum conditions (2×10^{-5} torr). The tank has nine independently powered and controlled 32 kW xenon arc lamps capable of providing 1.2 suns at the primary concentrator. Two types of primary concentrators were used: a fixed disk and an inflatable type. Multiple thermocouples were located outside the rhenium cavity. Details of the testing have been summarized in references 3 and 4.

First Concentrator

On April 17, 2000, efficiency tests were run at low temperature and high power. The rhenium receiver was not used and the output of the RSC was directed into a calorimeter. The crystal was held in place with eight spring loaded shoes, to allow for expansion, as shown in Figure 2(a). These tests are described in detail in Reference 4.
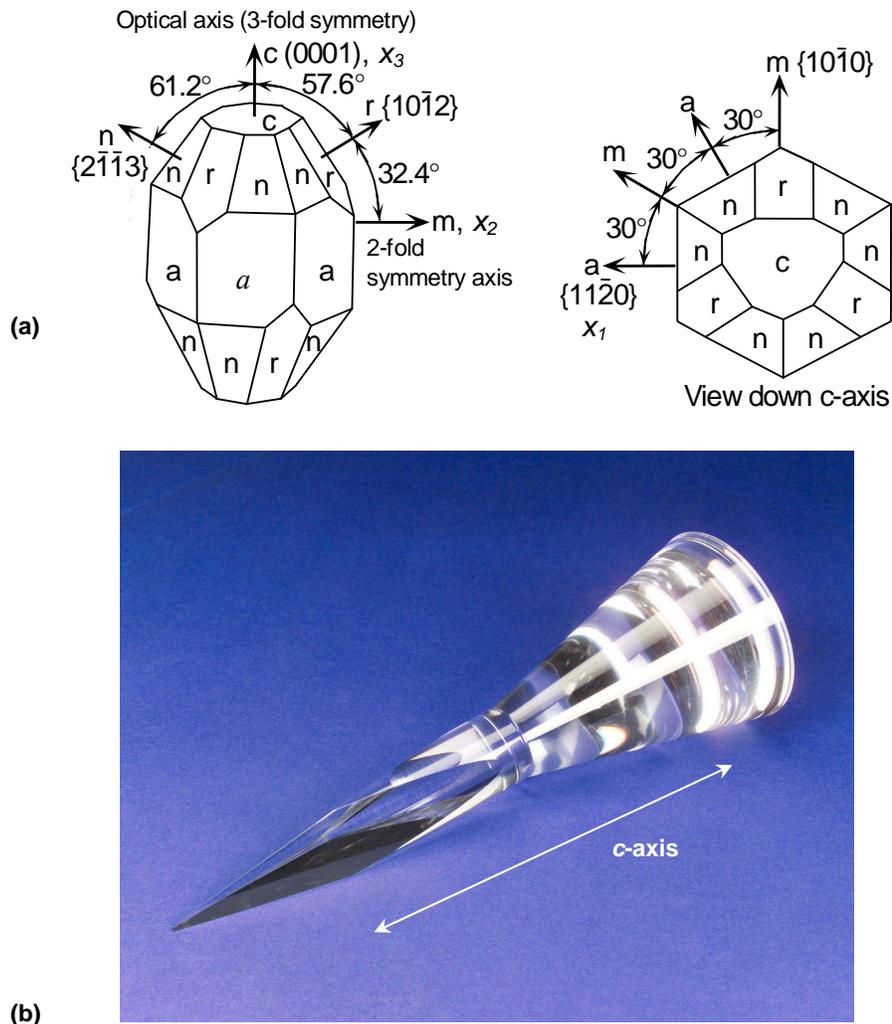

Figure 1.—(a) Sapphire crystal showing mineralogical and Miller index notation. The *c*-axis is a 3-fold symmetry axis, but sapphire is indexed as a hexagonal unit cell with *c/a* = 2.730; and (b) sapphire concentrator prior to testing.
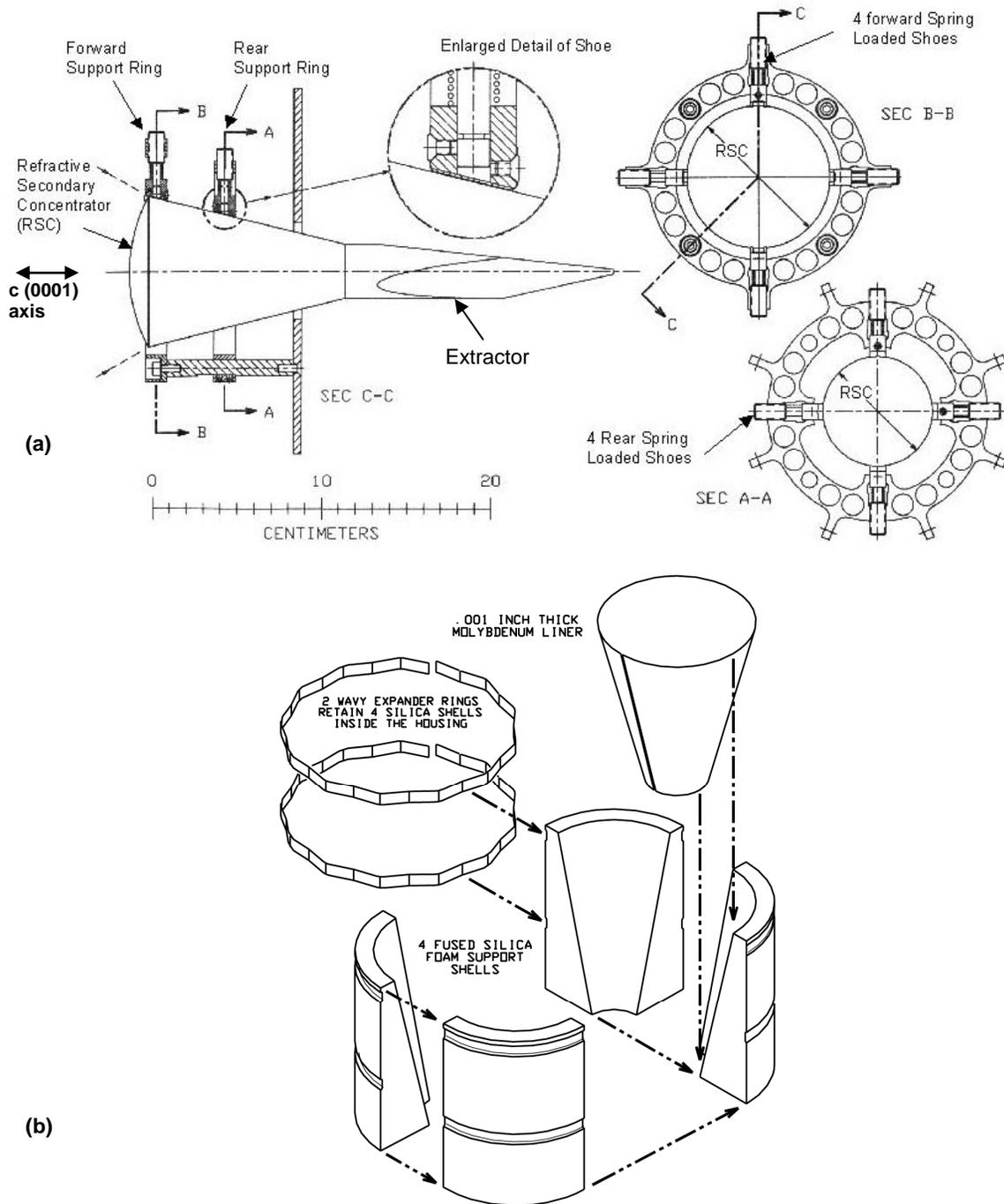
Figure 2.—Test assembly for (a) the first (exposed cone) and (b) the second (covered cone) RSCs.
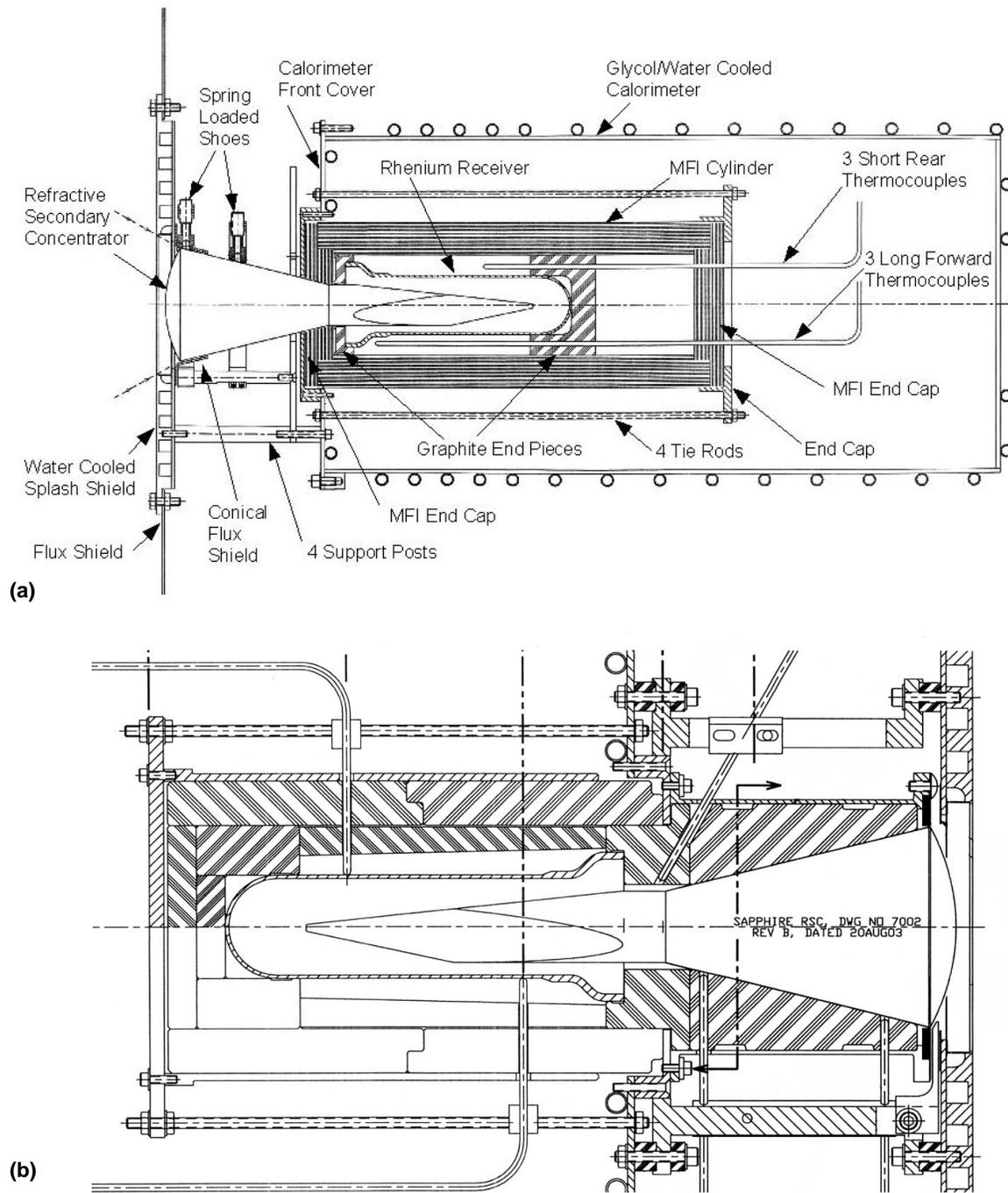
Figure 3.—Layout of the receiver, thermocouples, insulation and calorimeter for (a) the first and (b) the second refractive concentrator.

(a)

(b)
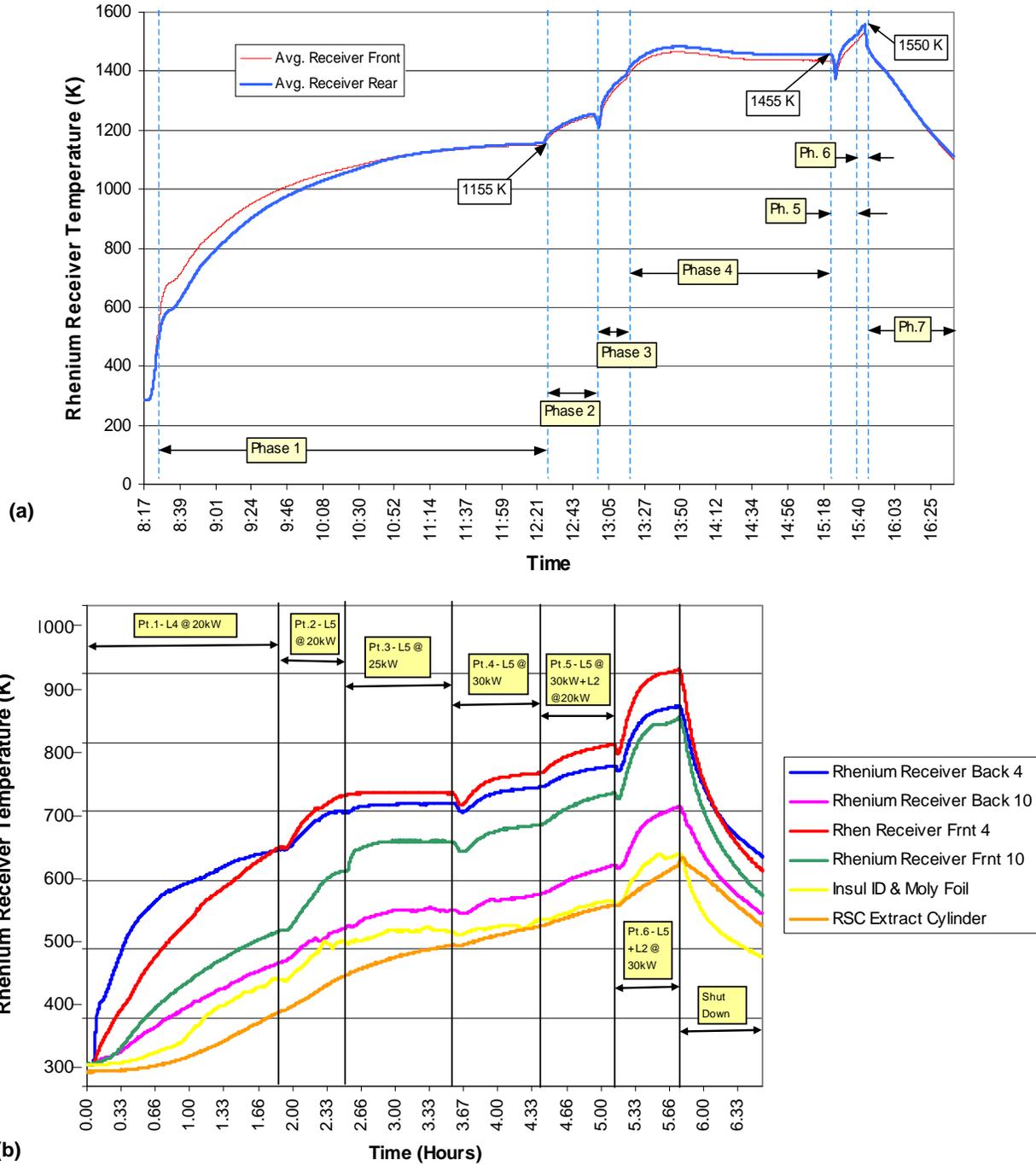
Figure 4.—Average temperature profiles of (a) the first RSC and (b) the second RSC. The dips at the start of phases 3 and 5 are due to short periods in which the solar simulator shutter was closed to allow ignition of additional lamps.

(a)
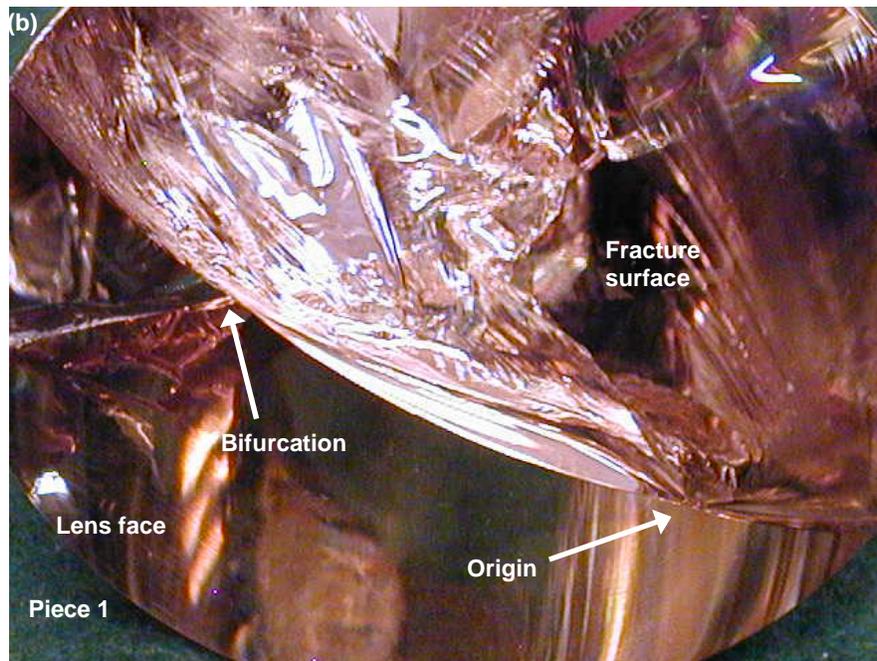
(b)

Figure 5.—(a) Overall view of RSC no. 1, the first solar concentrator, after testing. The lens diameter is 89 mm (3.5 in.) and the overall length is 284 mm (11.2 in.). (b) View of the fracture surface face of the bottom half (piece 1) showing the fracture origin and bifurcation that is located 44 mm away from the origin.

On August 30, 2001, two tests were run with the rigid primary concentrator—one at lower temperatures without the Re receiver and one at higher temperatures with the Re receiver. The high temperature test had an approximate maximum receiver temperature of 1300 °C (1573 °K) and an approximate front shoe temperature of 532 °C (805 °K), with a peak shoe temperature of 582 °C (855 °K) after shut down. The first indication of performance problems was an unexpected decrease in temperature as shown in the temperature—time profile in Figure 4. The test was shut down and cracks in the lens could be seen once the temperature cooled to ~982 °C. Upon inspection the crystal was observed to be cracked as shown in Figure 5.

Second Concentrator

On March 31, 2004, tests were performed with a new concentrator and holder that were designed to lower thermal gradients and minimize contact stresses. The new holder was made from a ceramic insulation fabricated to fit in a glove-like fashion around the RSC, with a molybdenum sheet between, as shown in Figure 2(b). In 2004 two tests were run—one test with an inflatable primary concentrator at a lower temperature and one at mid-temperature with the rigid primary concentrator and Re receiver. For the mid-temperature exposure the maximum receiver temperature was approximately 649 °C (922 °K) and the front shoe temperature was approximately 438 °C (711 °K). The crystal again failed. The temperature at failure was one-half of that in the first test, despite the use of more insulation and a lower temperature gradient. Figure 6 shows RSC no. 2 after removal from the test rig.
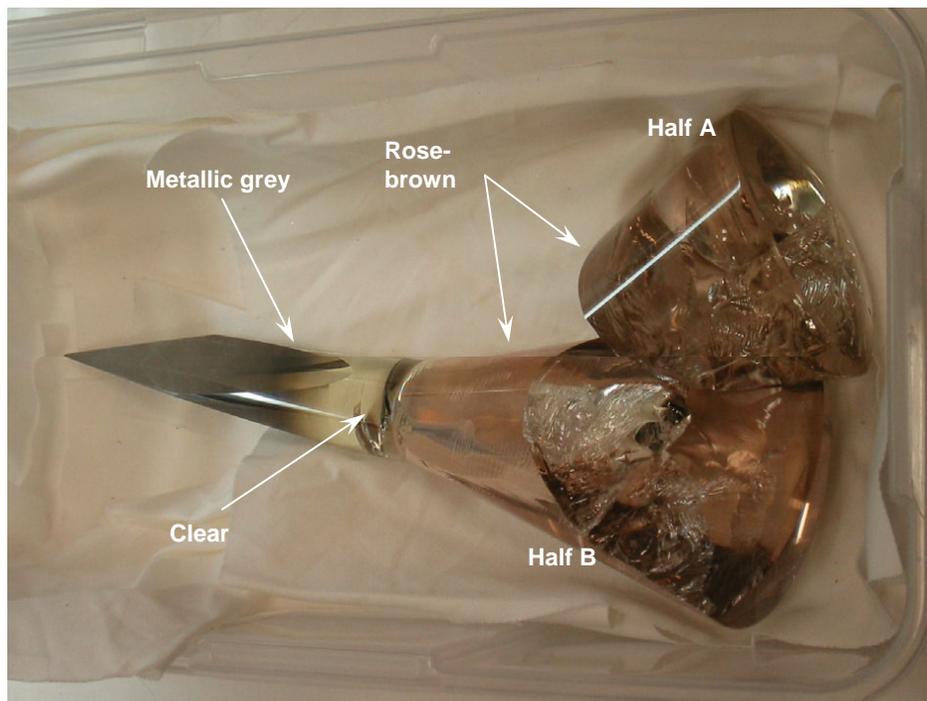

Figure 6.—RSC no. 2 after removal from the test rig. It has broken into two pieces. Cracks at the neck are also visible. The cracks in the neck and extractor are extensions of the main fracture in the cone body. The lens diameter is 89 mm (3.5 in.) and the overall length is 284 mm (11.2 in.).

General Observations

Both failed crystals exhibited similar features, including extensive cracking and internal discoloration in the conical region. As will be shown below, the primary fractures for both concentrators started at the rounded front lens faces and then propagated downward and inward through the concentrator. Both had classic brittle material type fractures. The main cleavage crack in both RSCs was radially aligned and x-ray diffraction indicated the main crack plane was coincident with the *m*-plane. The fracture origins were 3-dimensional surface flaws in both concentrators, but the flaws were not the same. Large twins were observed on the *r*-plane in one concentrator, but did not trigger the fracture.

First Concentrator

As shown in Figure 5(a), the lens face and cone are fractured near the mid-plane of the lens face and downward into the body to the extractor. There is a mixture of cleavage and conchoidal fracture and some crack bifurcations. As will be shown later, fracture started on the face of the lens and propagated downward into the cone body and extractor.

Besides the severe cracking, Figure 5(a) also shows that the cone region of the lens exhibits a rose hue when viewed on the cone sides, with thicker regions appearing darker than thinner regions. When viewed down the lens axis, a light-brown hue is exhibited in the uncracked regions, and rose hues in the severely cracked regions, probably from side light being reflected out the lens face. The rod region and a heavily cracked region of the cone are still clear.

Discoloration in sapphire can occur after high temperature heat treatments (usually greater than 1500 °C) if divalent cations are present (Ref. 5). The impurities need only exist at the part-per-million levels, and break the valence charge. Pink and red generally occur from Cr, however, color changes can occur from many common elements such as Ti, Fe, Ge, Si, Sn, Mg, Be, etc. Conventional chemical analyses methods such as x-ray energy dispersive spectroscopy (XEDS) is not sufficient to detect such impurities in sapphire. Use of secondary ion mass spectroscopy or laser ablation can yield accurate measurements on sapphire if the operator has sufficient experience (Ref. 5).

Discoloration can also occur after exposure to high-energy electromagnetic radiation, such as X-rays or ultraviolet radiation, as in this case. This phenomenon is known as "solarization," and is caused by the formation of internal defects, called color centers, which selectively absorb portions of the visible light spectrum. A separate investigation on RSC material chemistry has been published (Ref. 6).

Second Concentrator

As shown in Figure 6, the fracture started on the face of the lens and propagated downward into the cone body and extractor. The primary crack split the lens face and cone body near the mid-plane down to the extractor. Several *r*-plane bifurcations branch from the cone sides. The main crack rotated onto the *c*-plane after traveling ~15 mm into the extractor.

Besides being severely cracked, the cone region of the lens exhibits a translucent, lighter rose-grey hue as compared to the first RSC, with thicker regions appearing darker than thinner regions. The lighter color is likely a result of the lower temperature (and power) level. The end of the cone and the rod region just after the cone are clear whereas the remaining portion of the rod is an opaque dark gray.

Fractographic Analysis

First Concentrator

Figure 7 shows the four main pieces that concentrator no. 1 broke into after removal and some subsequent handling for the fractographic analysis. The origin is on the curved front face, about 20 mm away from the rim. There also is a large twin that extends diagonally all the way through piece 1 and which penetrates partially through piece 2. This twin was incidental and did not cause fracture.
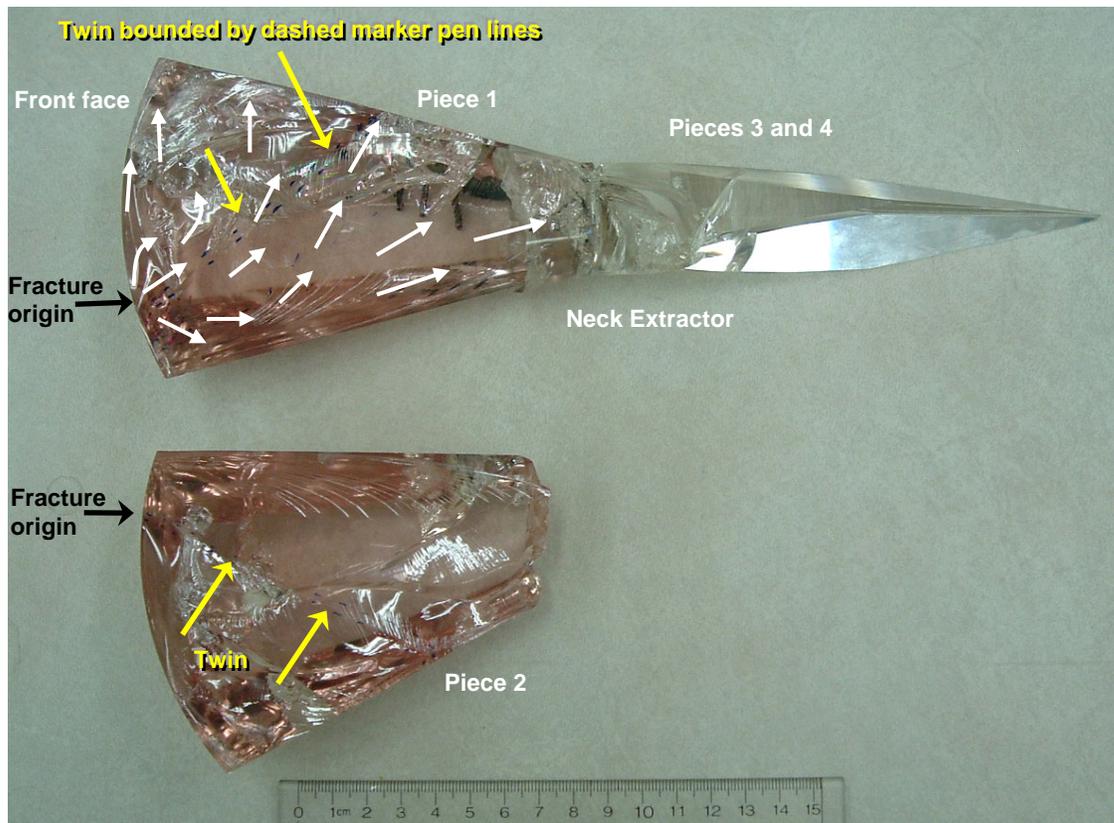
Figure 7.—Concentrator RSC no. 1 fractographic analysis. Fracture started from the fracture origin on the front face and propagated (white arrows) into the cone body and onwards to the neck and extractor. The initial main fracture was almost perfectly radial and close to the *m*-plane in orientation. All the cracking in the neck and cone body can be backtracked to the one fracture origin. An incidental twin ran entirely through piece 1 from the lens front face through to the cone side and out the back of the cone. One end was close to but not exactly at the fracture origin site (2.3 mm away). There were minor perturbations in the main crack when it reached the twin plane indicating that the twin was in the RSC before the crack ran through it. The twin was very shallow in piece 2. It ran from the lens face right through the side of the cone, but did not extend very far below the fractured surface. The insert shows how subsequent handling caused the extractor to split into two pieces that separated from the cone body.

Figure 8 shows a close-up of piece 2 revealing some of the classic fracture surface markings such as twist hackle, cleavage step hackle, Wallner and arrest lines. The fractographic analysis of single crystals is covered in detail in Reference (Ref. 7). It should be borne in mind when viewing this and the following figures that reflections and translucency make photographing single crystals difficult. In the examples below, some regions are shown with several views with different lighting to bring out various details. Failure occurred from the fracture origin site and extended parallel to the *m*-plane. The main crack plane emanating from the origin contains hackle lines that extend from the lens face to the extractor on one side. This is a distance of ~5 in., and the crack nearly cleaves the cone into two segments that attached at the extractor rod. On the other side of the origin, the crack cleaved the lens cone only to a depth of ~2 mm along the lens before splitting, moving off the *m*-plane and forming a confluence of cracks at a variety of angles.

There is a large density of cracks where the lens cone and extractor rod meet. The temperatures are large in this location and the section changes shape, so failure might be expected in this region, however, no origins could be identified and the observed cracking was the result of the main crack front reaching this region and being redirected and branched. Also, no cracks emanated from the support shoes on the cone body sides, where a perturbation in the temperature distribution might have occurred.
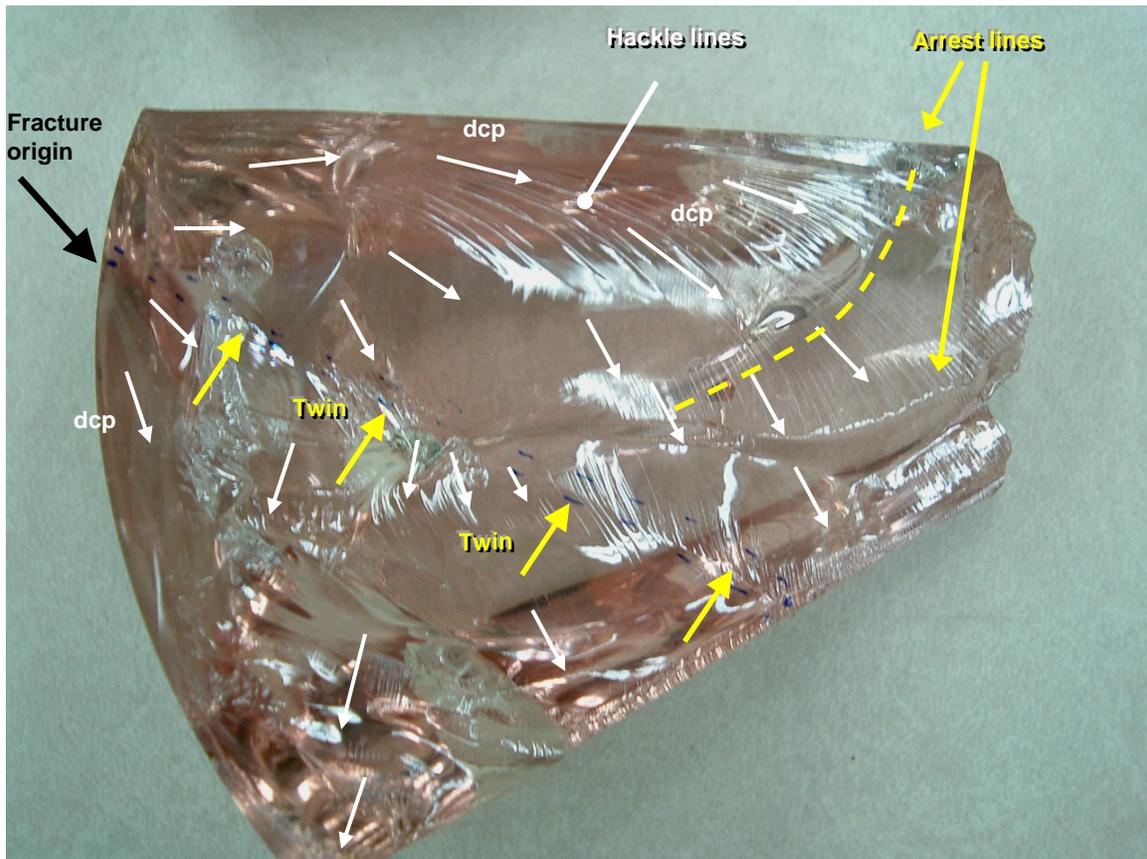

Figure 8.—Piece 2 of RSC no. 1. The small white arrows show the local direction of crack propagation (dcp) as identified by hackle lines, Wallner lines (not labeled), and arrest lines. These facilitate the determination of the crack propagation direction and the fracture origin. The twin runs diagonally across this view as marked by yellow arrows. Its left end comes very close to but is not coincident with the fracture origin. The main crack was perturbed slightly when it traversed across the preexisting twin.

Figures 9 to 12 show that the failure origin is on the lens face, about 20 mm away from the rim. These views were taken with different lighting at different angles. The origin is a large, partially formed Hertzian cone crack, that extended from one of two partially polished impact divots or "bruises" measuring ~ 0.1 and ~ 0.2 mm in diameter, as shown in Figure 12. The cracks associated with the bruises are quite large, ~ 0.5 mm, and the damaged region can be seen with the unaided eye. Contact damage usually has two forms depending upon the sharpness or bluntness of the offending impactor (Ref. 7). Sharp impactor contact damage usually has a small concentrated damage crater with a star like array of cracks radiating outwards. Blunt impactor damage has a conical or ring shape. Often it may be a partial ring shape such as shown in Figures 10 and 11. From the size of the ring crack, it may be deduced that the impact object had a diameter greater than 0.5 mm.

The Hertzian crack likely formed due to impact with a hard blunt object during the grinding or early polishing steps. As Figure 12 shows, final polishing created some microscractches around the bruises. These would not have been present if the impact had occurred *after* the final polishing phase. Better care would have eliminated this failure source.

In addition to the bruises, large remnant scratches from the rough machining were noted on the lens faces, Figures 10 and 11, but also on the shaft, Figure 13. Another scratch approximately 2.3 mm from the rim on the lens face extends along nearly ¾ of the perimeter and can easily be seen with the unaided eye, Figure 14. Also apparent are some semi-polished chips on the edge between the lens face and the cone, as shown in Figure 15. Ideally, better machining and polishing should be performed. Poor polishing, such as that observed, is referred to as a "short finish" and generally results in a very large variation in the measured strength (Ref. 8).
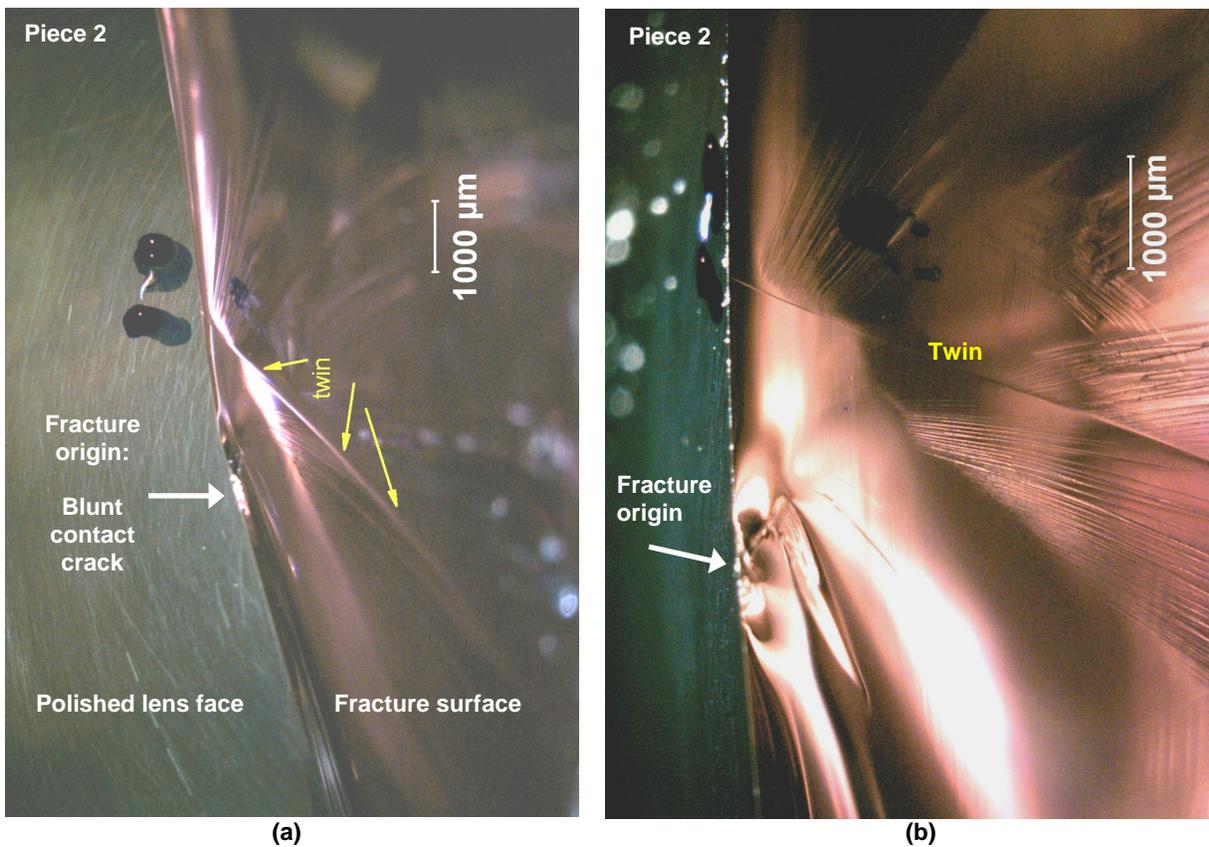

Figure 9.—Close- up views of piece no. 2 of RSC no. 1 with about the same orientation as in Figures 7 and 8. Minor polishing scratches are revealed by the lighting in (a). (b) is a close up of (a).
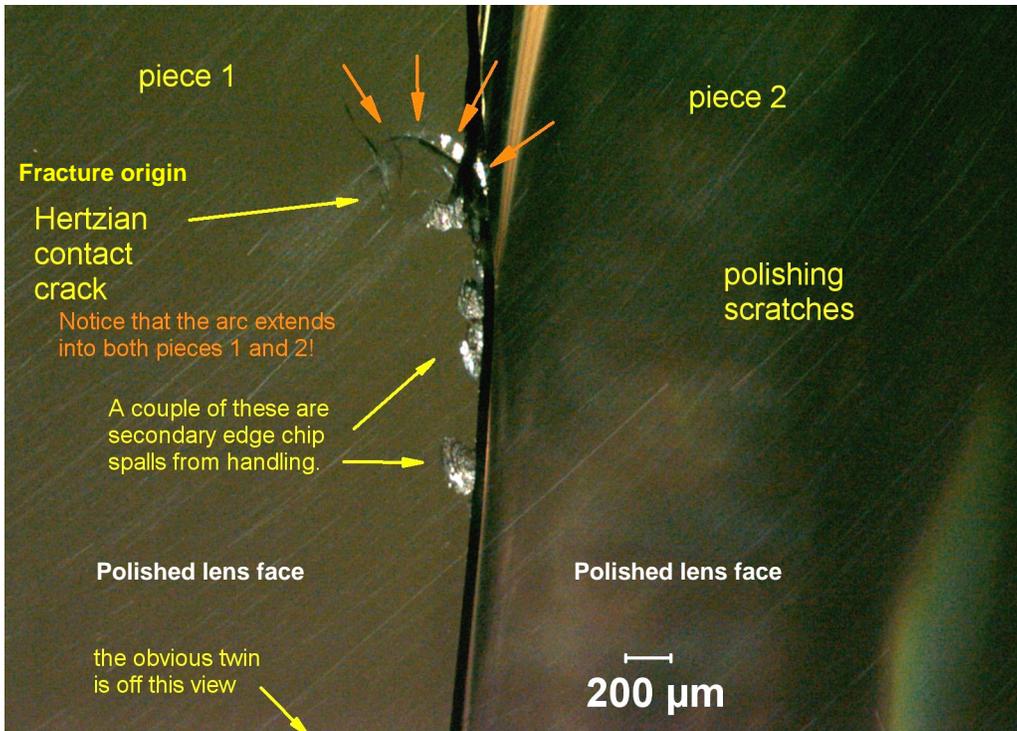
Figure 10.—This view shows the curved polished face of pieces 1 and 2 of RSC no. 1 held together at the origin site. The orange arrows highlight the Herztian (blunt impactor) contact crack.
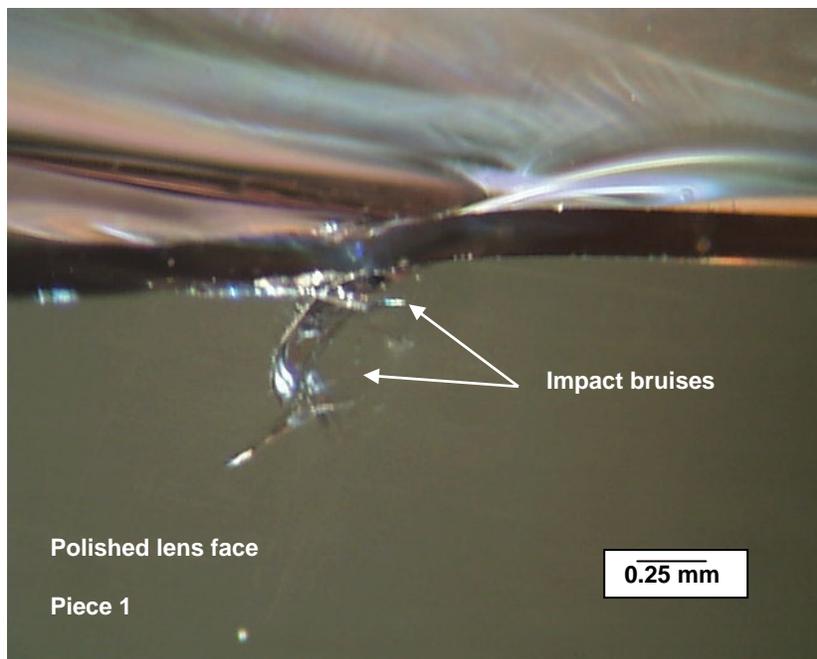

Figure 11.—View of piece 1 of RSC no. 1 showing cracks extending from bruises on the lens face. The sites of the impact bruises are marked in this view, but they are more obvious in the next figure which has different lighting.
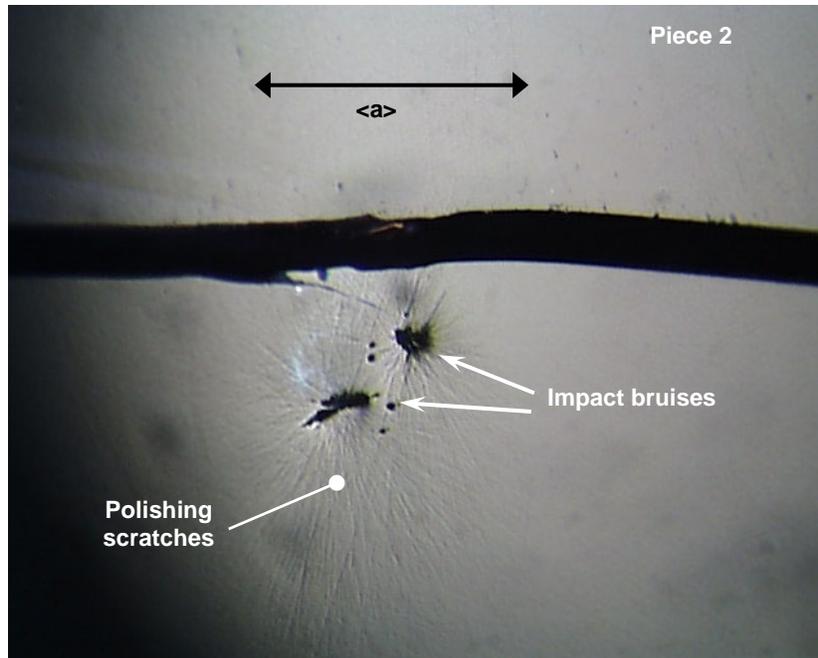
Figure 12.—Surface lighting of the bruises revealing polish scratches in the polished face of RSC no. 1. The residual scratches that radiate from the contact sites imply that the impacts occurred prior to the final polishing of the face. Final polishing caused micro scratches to radiate outward from the damage sites.
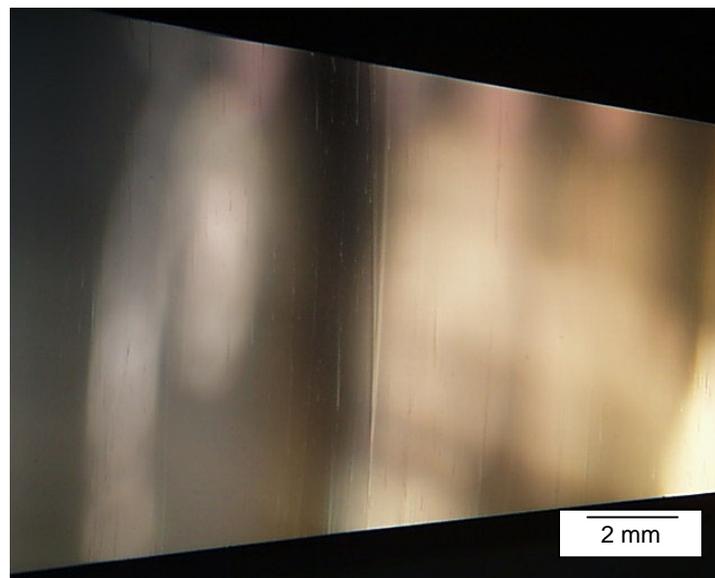
Figure 13.—Grinding marks along extractor shaft of RSC no. 1.
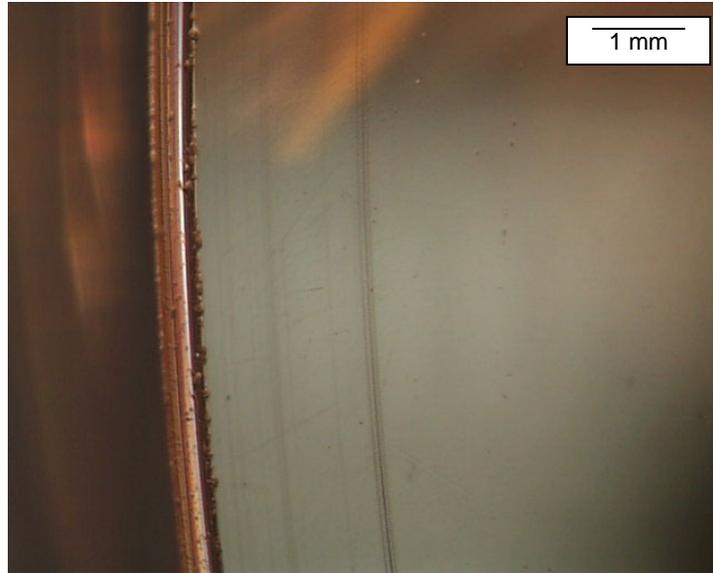
Figure 14.—Grinding damage and scratches on the lens face near the rim of RSC no. 1.
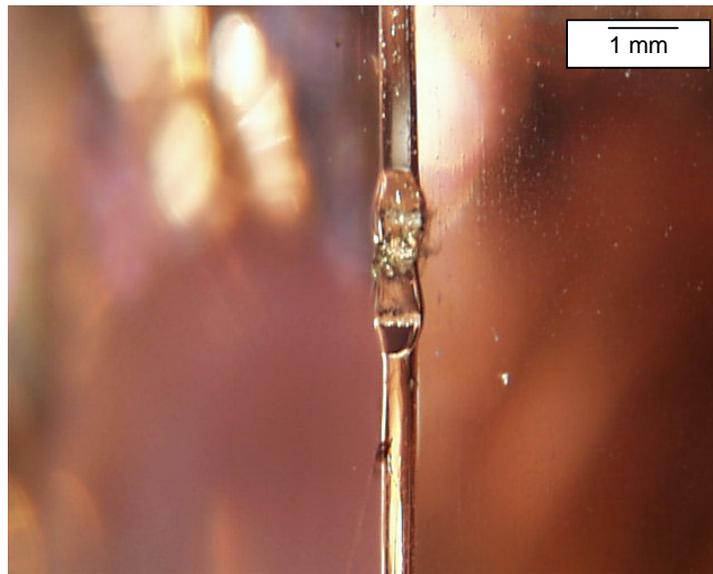
Figure 15.—Chips on the rim of the lens of RSC no. 1.

The twin that was observed running through RSC no. 1 is shown in Figures 7, 8 and 16, but it appeared to have been incidental. It could not be determined where it initiated. It was more obvious in piece 1 and it penetrated completely through the piece. It was seen over all surfaces with the naked eye. It extends only partially into piece 2. It is also visible on piece 2 primarily by how it affected the main crack propagation. Additional twins that were detected in the front face of piece no. 1 are shown in the Appendix.
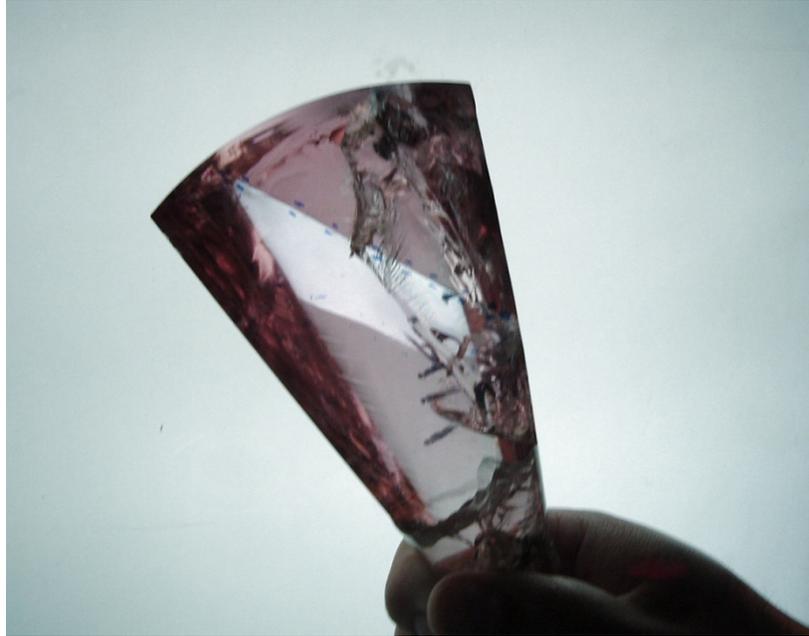
Figure 16.—A prominent twin (the light colored band) ran through the body of piece 1 of RSC no. 1. This is a view of the piece through crossed polarizers.

Second Concentrator

Figure 17 shows fractured RSC no. 2, which was intentionally sliced after the test in order to facilitate chemical analysis and fractographic examination. Hereafter the two halves of the conical body are referred to as half A or half B as shown in the figure. The main crack plane emanating from the origin contains twist hackle and cleavage step hackle that extend from the lens face to the rod neck and extractor. Once entering the rod extractor, the crack turned onto the c-plane, nearly cleaving the rod.

The crack path down the cone is parallel to the m-plane on one side and ill-defined on the other, and separates the cone into two halves. At ~17 mm from the origin along the side, the crack bifurcated once onto the r-plane. This bifurcation was followed by several others, one of which exited the cone, causing a portion of the lens to separate diagonally from the rest of the cone. Along the lens face, the crack extended along the r-plane until the middle of the lens, where it propagated in a conchoidal fashion. The first bifurcation occurred onto an m-plane at ~17 mm along the face. This was followed by second and third bifurcations at ~22 and ~30 mm (shown later in Figure 22(a)). The third bifurcation extended to edge of the lens, whereas the first two stopped within the concentrator.

There was a single fracture origin on the lens face that was located only 0.5 mm away from the rim bevel and 1.3 mm away from the cone side wall as shown in Figures 17 and 18. It is not known whether this site was coincident with a shoe contact site as shown in Figures 2 and 3. On half B the origin is clearly identified as a large curved scratch. Close up views of half B are in Figures 19 and 20 which show the curved scratch in more detail.

Figure 21(a) and (b) shows a variety of grinding irregularities in the lens front face and bevel.

The matching half A of concentrator 2 is shown in Figures 22 to 25. The crack from the scratch is less clearly evident and attention is drawn to what appears to be a pit at the origin site. No trace of the apparent pit existed on half B. The "pit" is probably secondary chipping after the main fracture occurred or it may have been a small initial pit that was enlarged by secondary chipping. The scratch is the primary flaw.

In addition, occasional, large remnant scratches from the initial rough machining stages can be noted on the lens, rod and cone, as shown in Figures 26 and 27. Several other features in the vicinity of the origin were also detected as shown in Figure 28, but they appeared to be incidental micro twins.
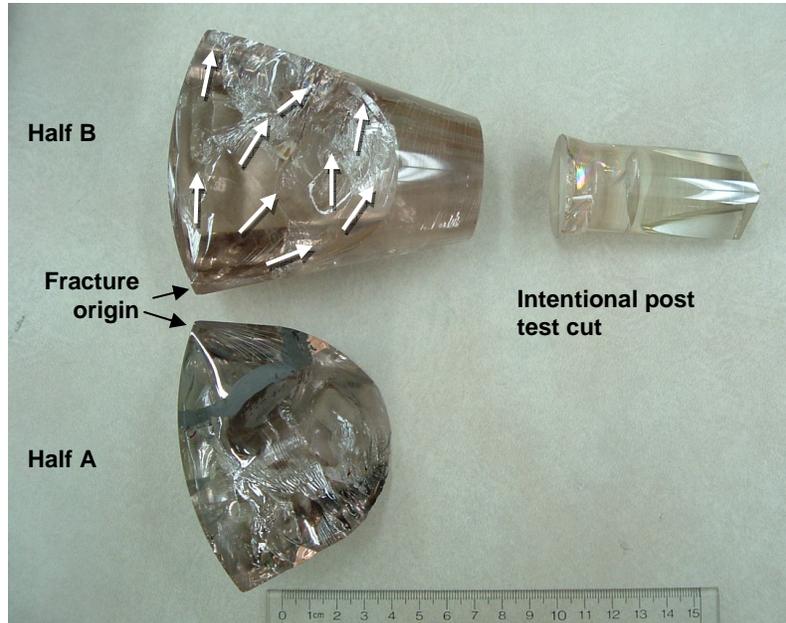

Figure 17.—Concentrator 2. The white arrows show the direction of crack propagation.
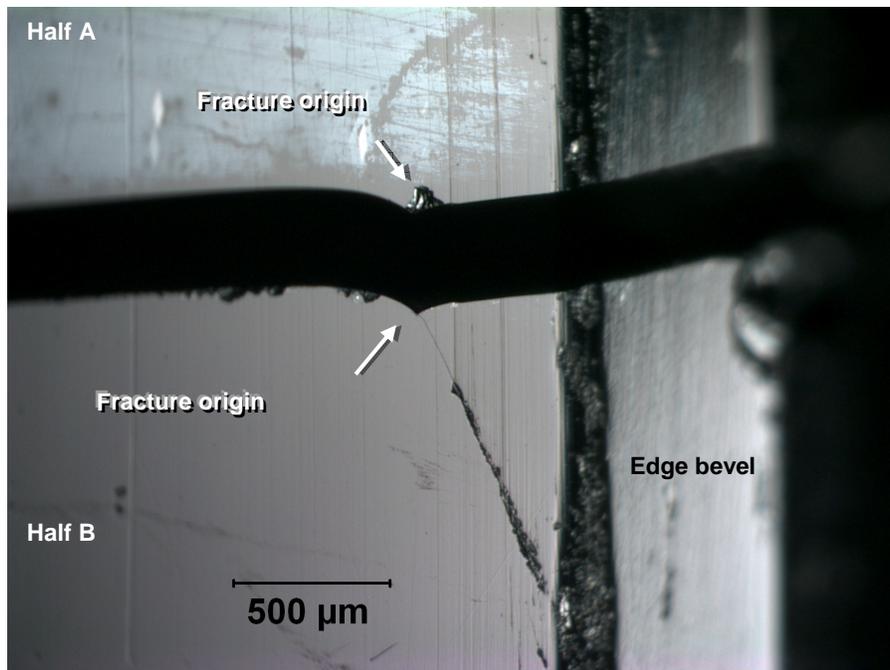

Figure 18.—View of curved forward face of RSC no. 2. Fracture started from a curved scratch best seen on half B on the bottom. Note the secondary chipping on both halves along the main fracture plane.
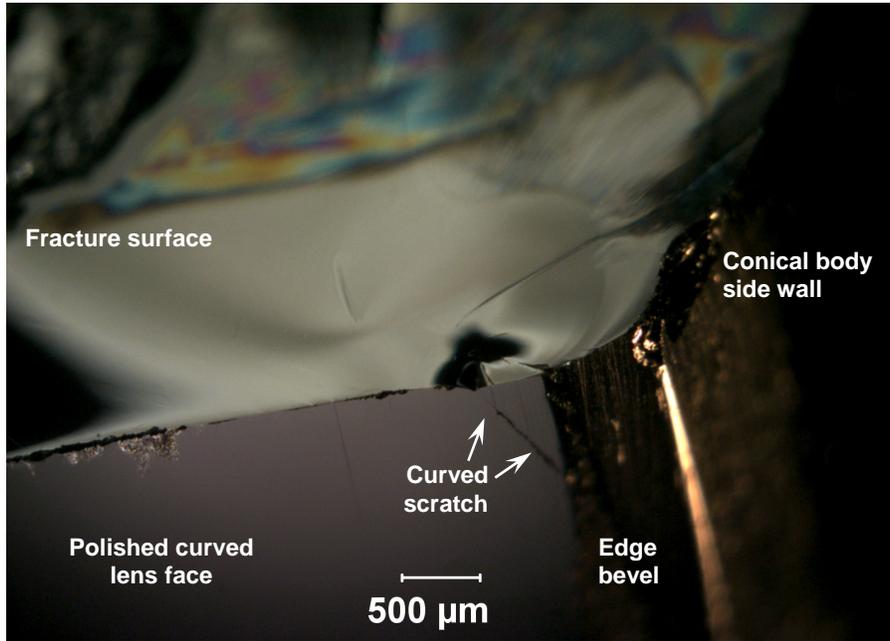
(a)
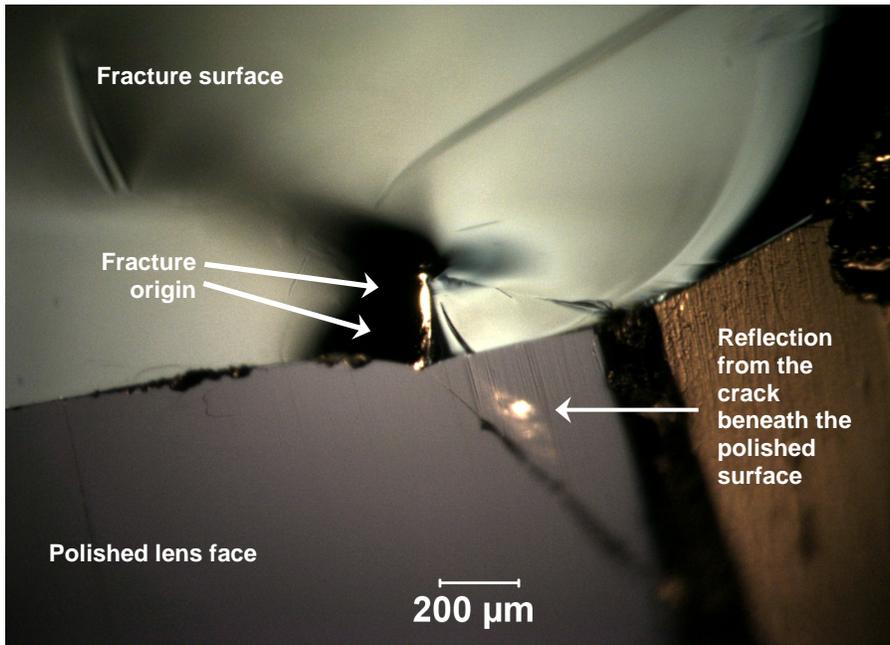
(b)

Figure 19.—Stereo optical microscope views of half B of RSC no. 2. The piece has been tilted so that both the fracture surface and the polished curved lens face can be seen. (b) is a close up of (a).
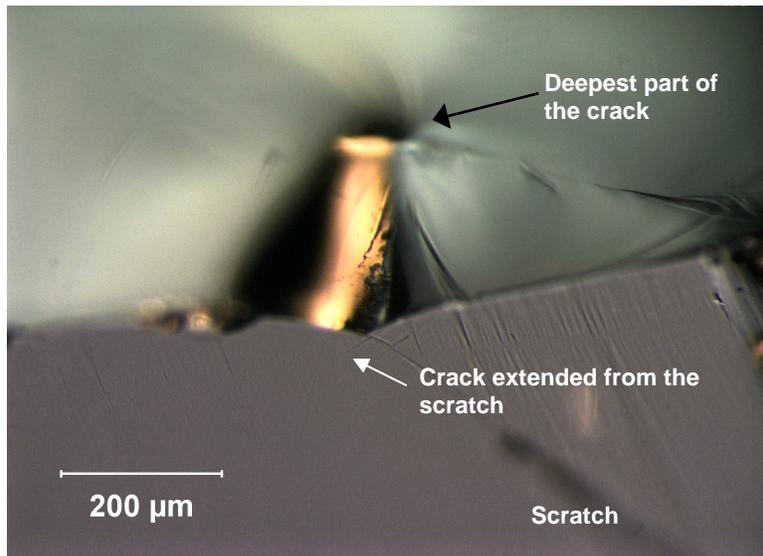
Figure 20.—Detail of the fracture origin of RSC no. 2, in half B. A crack extends from the scratch region (out of focus in this view) which is characterized by tell tale short lateral spall cracks. The crack created underneath the scratch extended upwards and curved to the left in this view (small arrow). The crack penetrates at least 250 µm deep beneath the polished surface into the lens body. Lens fracture started from the deepest point of the crack indicated by the black arrow. In this view, light reflections from the subsurface curved crack face cause shadows and bright reflections.
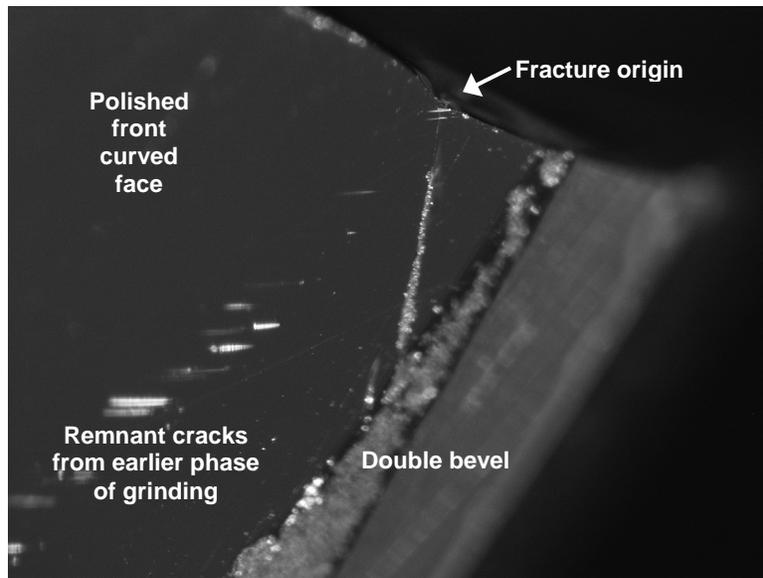
(a)
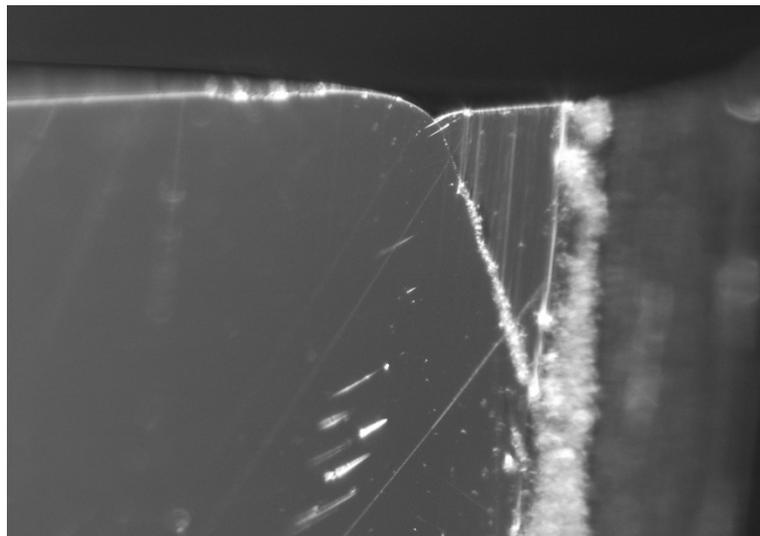
(b)

Figure 21.—Two views of the same area of the polished face and edge
bevel of half B of RSC no. 2 revealing additional irregularities
besides the curved scratch. Notice how adjusting the lighting in (b)
can bring out some scratches that are not visible in (a).
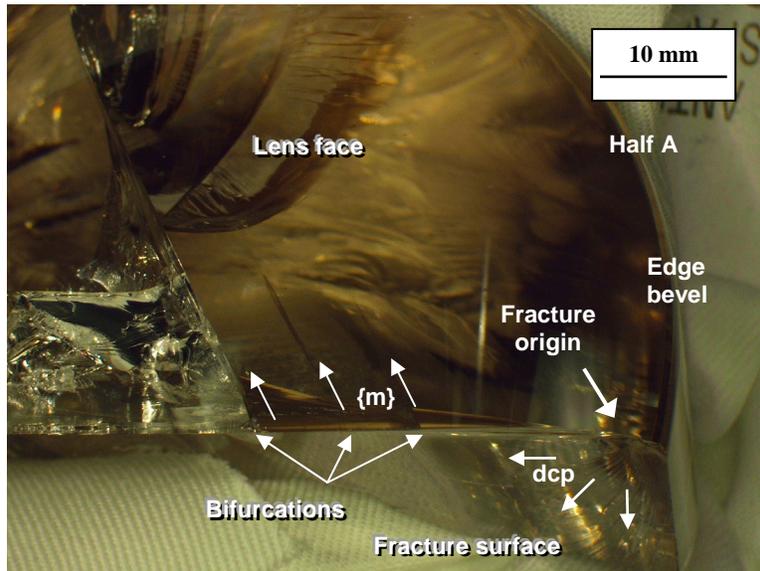
(a)
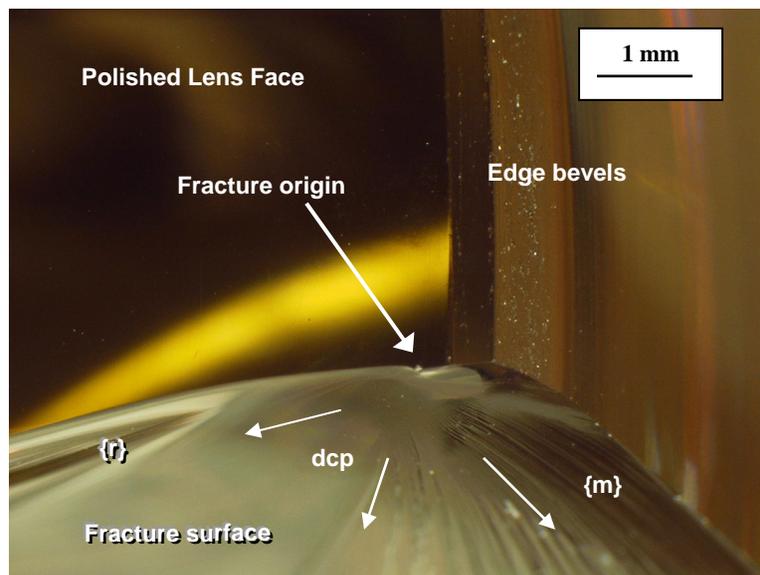
(b)

Figure 22.—Views of the fracture origin area in half A of RSC no. 2
showing both the fracture surface and the polished front surfaces.
Bifurcations onto the {m} plane are evident in (a). The first two do not
extend very far into the body, but the third causes a main crack to
form all the way through the body. (b) shows radiating hackle lines
on the fracture surface that point back to the origin site. "dcp" is
direction of crack propagation.
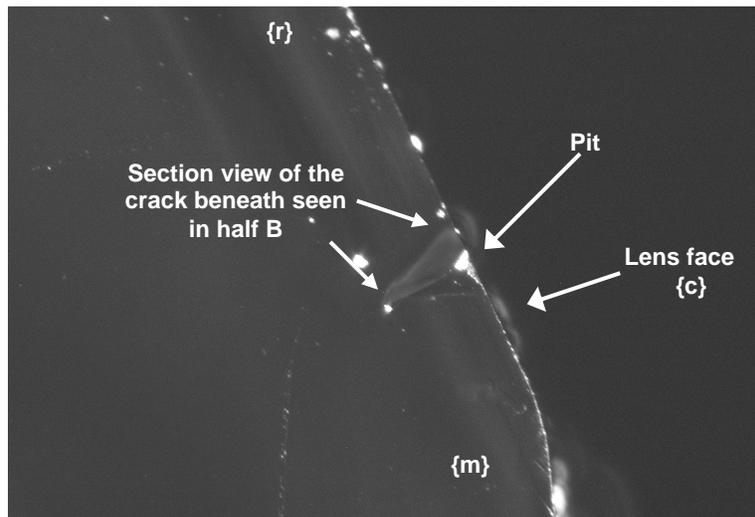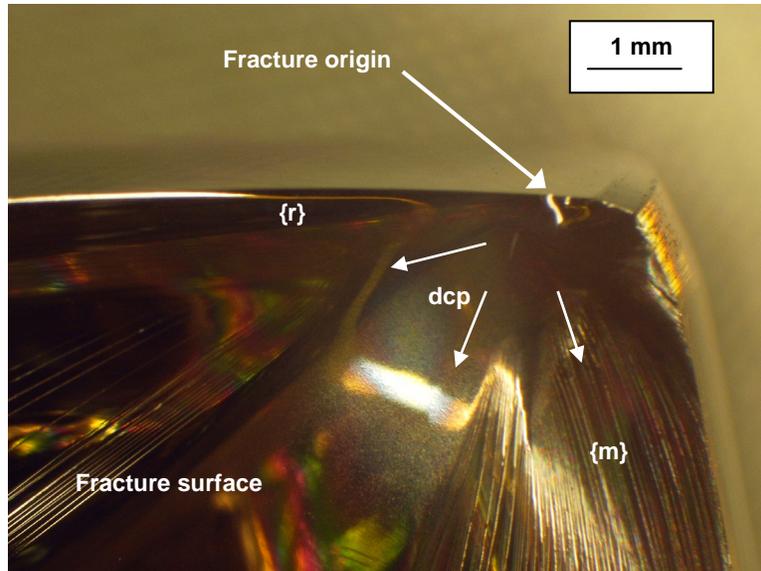
Figure 23.—View of fracture surface of half A of RSC no. 2 showing hackle lines that formed on {r} and {m} planes on either side of the origin.
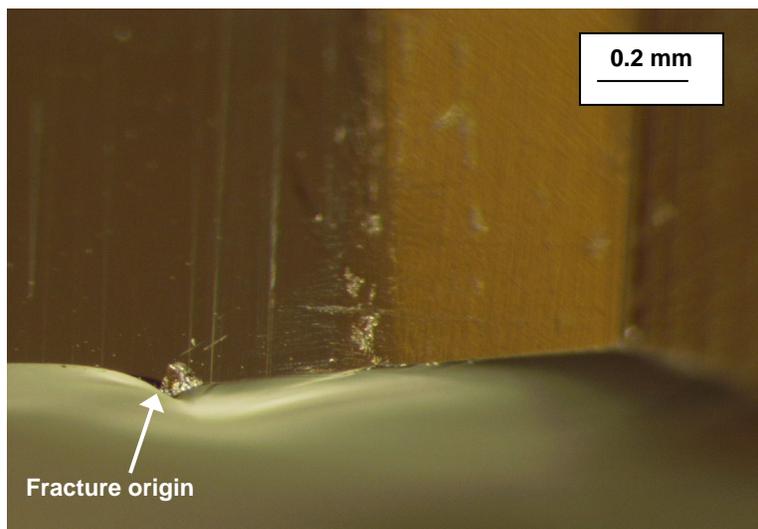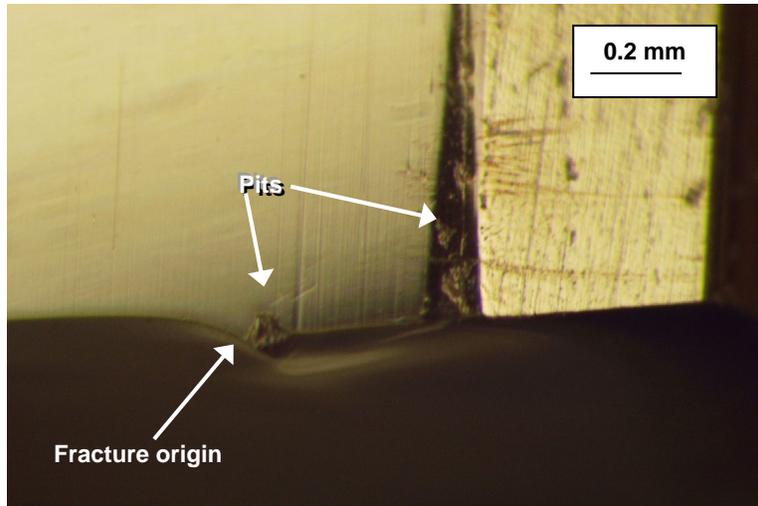
Figure 24.—Two views with different illuminations of lens face of half A of RSC no. 2 showing surface scratches, pits, and the fracture origin site.
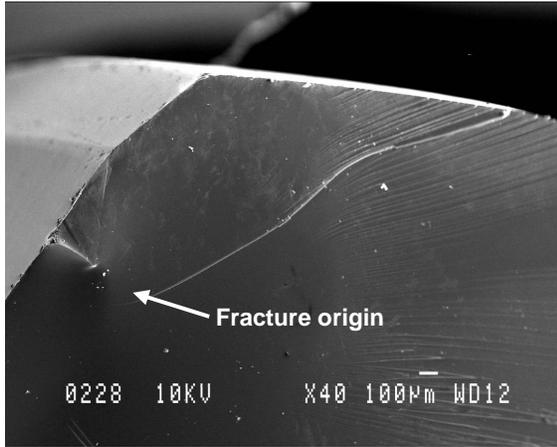
(a)
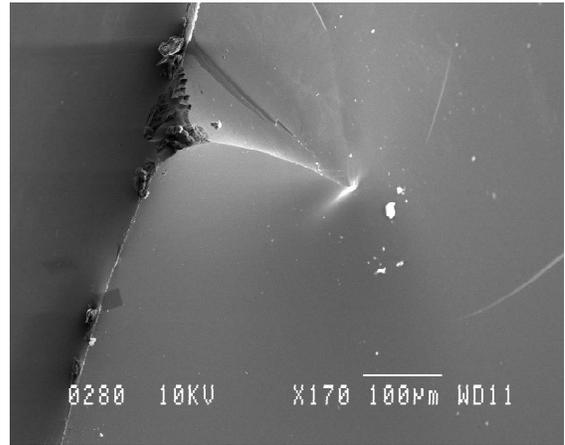
(b)
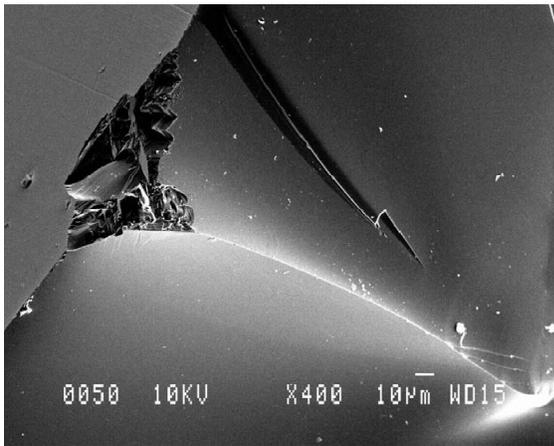
(c)
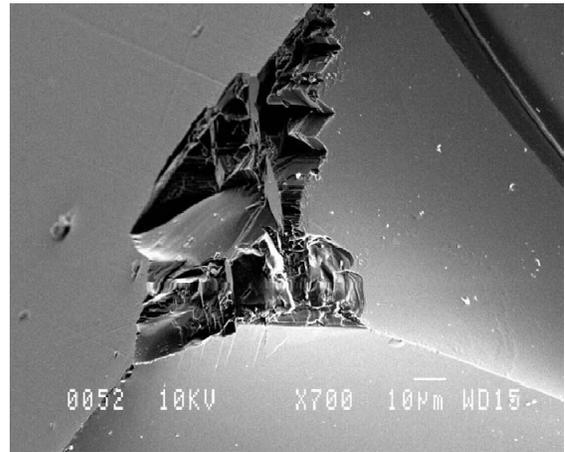
(d)

Figure 25—SEM close-up views of the origin in half A of RSC no. 2. (b) to (d) are close up views. The origin is the crack that penetrated beneath the polished surface. The "pit" is probably secondary chipping although genuine pits were noted elsewhere in the vicinity.
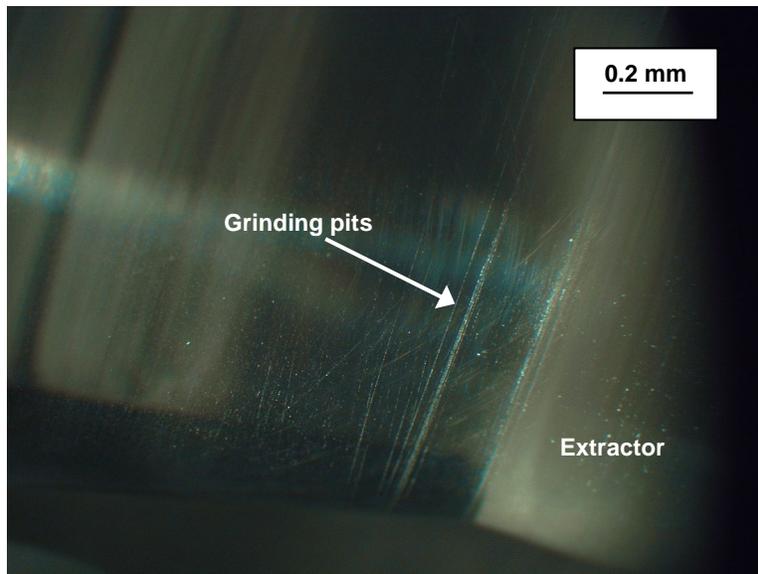
Figure 26.—View of lens cone and rod of RSC no. 2 showing surface scratches (grinding damage) prior to testing.
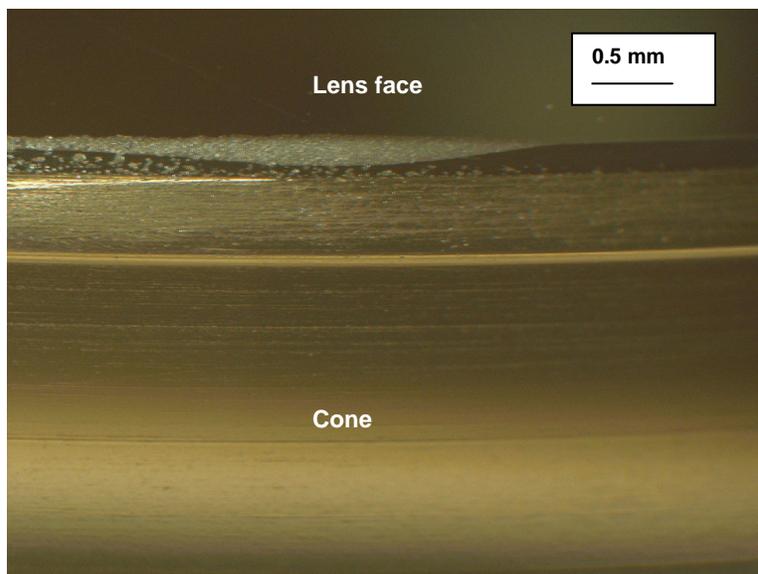
Figure 27.—View of RSC no. 2 cone and bevel showing heavy pitting and surface scratches (grinding damage) prior to testing. Notice the two step uneven bevel.
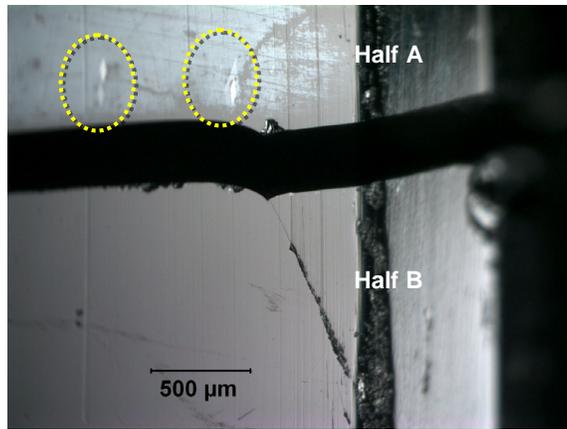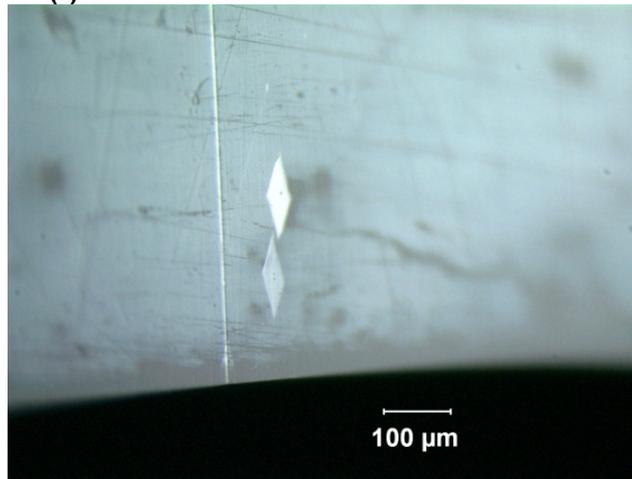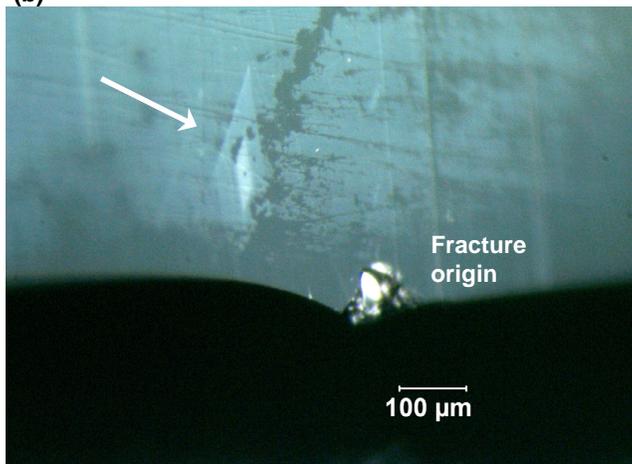
Figure 28.—Odd features detected on or just underneath the surface in half A of RSC no. 2 near but not actually at the fracture origin site. (a) shows the overall origin area with arrows marking the strange features. (b) and (c) are close up views.

Estimation of the Failure Stress

First Concentrator

Quantitative fractographic analysis may be used to estimate fracture stresses in brittle materials (Refs. 7, 9 to 11). The crack radiates outwards at high speeds once unstable fracture occurs. Telltale markings form on the fracture surfaces at distances from the origin that may be correlated to the stress in the part at fracture. The distance to the first crack branch (bifurcation) also depends upon the stress. These distances may be measured and used to estimate the fracture stress. This is a well established procedure for glasses and polycrystalline ceramics, but is less commonly used for complex single crystals. The estimates in this section for the sapphire lenses are only rough approximations for reasons discussed below. Strong thermal or stress gradients and residual stresses can create deviations from the relationships. Nevertheless, they provide a check on the finite element analysis predictions of the stresses present in the lenses.

The nominal local fracture stress associated with tension and uniaxial or biaxial flexure can be estimated from (Refs. 7, 9 to 11):

$$\sigma_f = \frac{A_j}{\sqrt{r_j}} \tag{1}$$

where σ_f is the remote fracture stress and A_j is a particular constant corresponding to a particular boundary with radius r_j , where j is m, h, or b for mirror, hackle or branching as shown in Figure 29, which shows an idealized schematic for a surface flaw. Equation 1 is valid for uniform steady state stress fields.

In RSC no. 1, bifurcation occurred at ~ 44 mm from the origin across the top round polished face, as shown in Figure 8, with a nominal angle of 52 °.

The value of A_j is a function of the material's microstructure and to a lesser degree of the specific conditions of failure (i.e. the stress state and the severity of stress gradients) (Refs. 7 and 12). Application of this approach to single crystals such as sapphire is complicated by the tendency for cracks to propagate on specific planes, and ideally the constants should represent the same crystal orientation and stress state. Unfortunately specific values of the branching constant A_b for the m- and r-planes of sapphire are not available. However, several estimates of the branching constant were obtained as follows.

Polycrystalline alumina subjected to biaxial flexure has a value of 7.4 MPa√m and for coarse grain alumina subjected to uniaxial tension, a value of 7.3 MPa√m has been reported (Ref. 7). In addition, the branching constant was evaluated from data on sapphire uniaxial flexure specimens with a-plane cross sections that were tested previously (Ref. 8). The results are shown in Figure 30. The specimens exhibited branching from the a-plane to the r-plane (see Fig. 26 of Ref. 8)). Besides calculating a mean value from eq. (1), linear regression of the following forms of eq. (1) was used to make estimates:

$$\log \sigma_f = M \log r_b + \log A_b \tag{2}$$

$$\sigma_f = A_b r_b^{-0.5} + \sigma_{th} \tag{3}$$

where σ_{th} is interpreted as either a threshold stress for branching or a residual stress (Refs. 7 and 13). Equations 1 to 3 yield A_b of 7.2 ± 0.6, 7.9 ± 1.5, and 7.0 ± 0.3 MPa√m for the sapphire respectively, with M = -0.49 and σ_{th} =11 MPa, as shown in Figure 30. These results compare well with those in (Ref. 7), implying a relatively constant value for alumina. The presence of a slight residual stress is not surprising, considering the grinding damage observed on the specimens via X-ray topography (Ref. 8), but this would be very shallow. During measurement of the branch lengths, several specimens were observed to exhibit fracture on the r-plane and bifurcation onto another r-plane. When the principal stresses were resolved on the r-plane, similar A_b resulted.
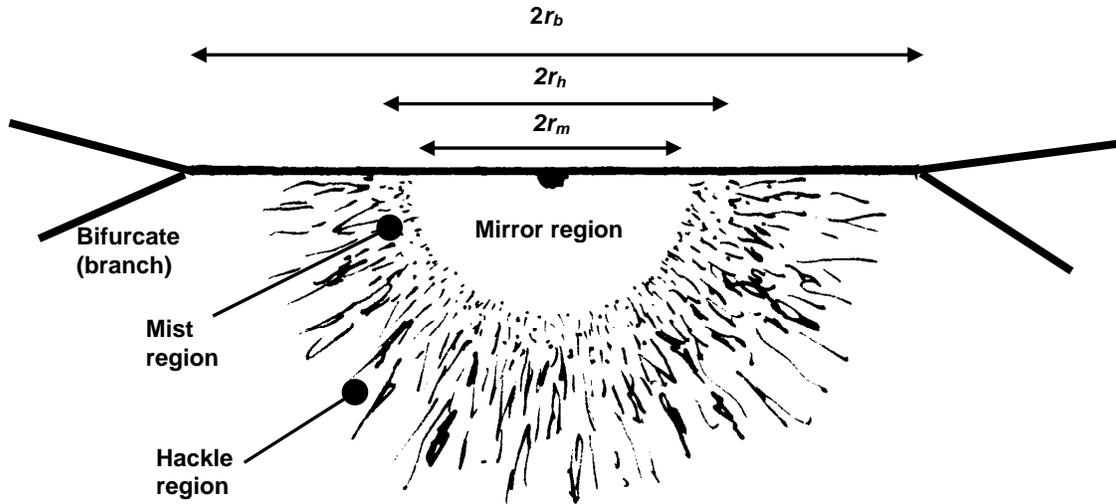
Figure 29.—Idealized regions and boundaries formed around a failure origin on the surface of a part that was exposed to uniform tension stress. The distance r_m is the radius of the boundary for the onset of mist, the distance r_h is the radius of the boundary for the onset of hackle, and the distance r_b is the radius of the boundary for the onset of branching. Problems in interpreting single crystal fracture mirror markings often force one to use the branching distance for quantitative stress estimates.
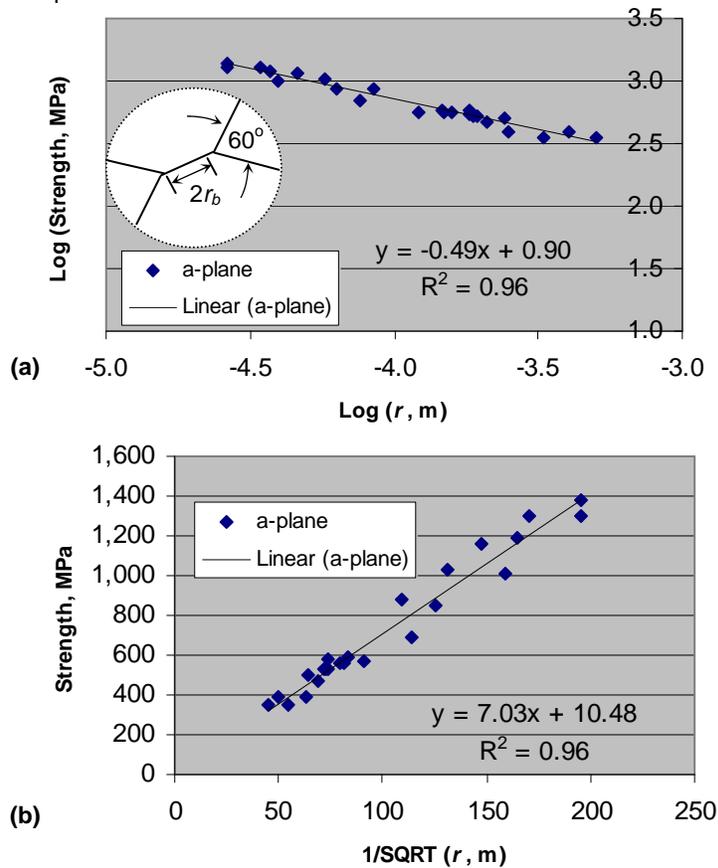
Figure 30.—Room temperature fracture strength as a function of branching length for the *a*–plane of sapphire tested in four-point flexure: (a) fit to Equation (2) and (b) fit to Equation (3). Strength data from Reference 8.

Assuming that the room temperature fracture constants are applicable, the 44 mm bifurcation distance used with Equation (3) implies a stress of only ~44 MPa. This is much less than the 250 MPa or larger strengths exhibited by well polished sapphire tested at low temperatures (Ref. 8). This very low stress estimate is consistent with the observation that the contact crack origin was moderately large. Large cracks require very little stress to trigger fracture.

Localized heating from the bruises should not have played a role because radiant heating of sapphire is not too sensitive to the surface finish.

Second Concentrator

Both of the crack fronts running along the *m*-plane (Fig. 22(b)) and *r*-plane (Fig. 22(a)) bifurcate at ~17 mm. Figure 22(a) shows several short bifurcations that are in a row, but these all arrested after a short propagation into the cone. The first significant bifurcation occurred at 30 mm from the origin. The bifurcation distance of ~17 mm combined with $A_b = 7.0$ MPa$\sqrt{m}$ and equation 3 implies a fracture stress of ~65 MPa. The larger distance (30 mm) gives a stress estimate of 51 MPa using equation 3. This also is a very low stress, but again, these estimates are supported by the observation that the flaw at the fracture origin was rather large and deep.

Stress Analysis

In order to understand the stress state in the RSC and design better RSC systems, finite element analyses were performed by using the single crystal thermal and elastic constants (Ref. 14). The resulting thermal and stress profiles are shown in Figures 31 and 32 for the first concentrator and indicate a maximum principal tensile stress of 57 MPa at the rim of the front lens face of the concentrator where the a- and *m*-axes exit, near the actual failure. This is in reasonable agreement with the value of 44 MPa based on fractographic measurement.

For the second concentrator, FEA modeling (covered cone design, 1200 °C) shown in Figures 33 and 34 indicates somewhat lower tensile stress of about 20 to 25 MPa on the lens face. Peak stresses up to 52 MPa occur just before the transition from the lens cone to the extractor rod.

As noted previously, the radial cracking suggests that tensile hoop stresses at the rim caused fracture in both concentrators. The origins were also located near the rims, where shielding and clamping may alter the temperature profiles relative to those estimated by the FEA analyses based upon the assumed boundary conditions. Better modeling with more realistic boundary conditions may give improved stress estimates in the front face rim regions.
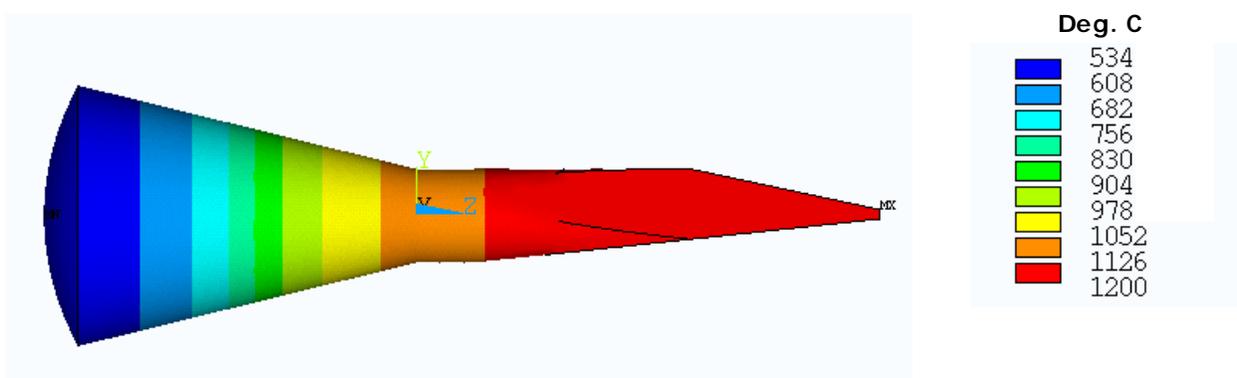

Figure 31.—Temperature distribution in sapphire crystal for receiver temperature of 1200 °C with exposed cone design.
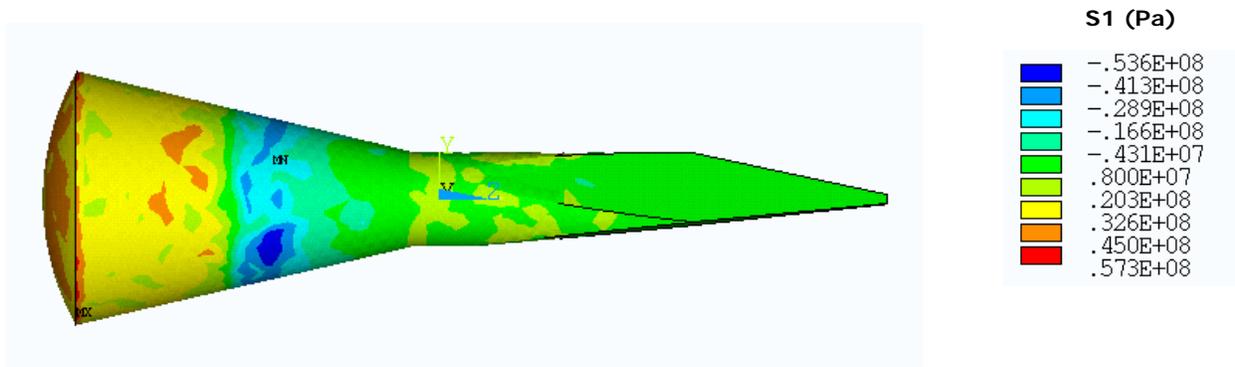
Figure 32.—First principal stress distribution in sapphire crystal for receiver temperature of 1200 °C with exposed cone design. Stress results are in Pa.
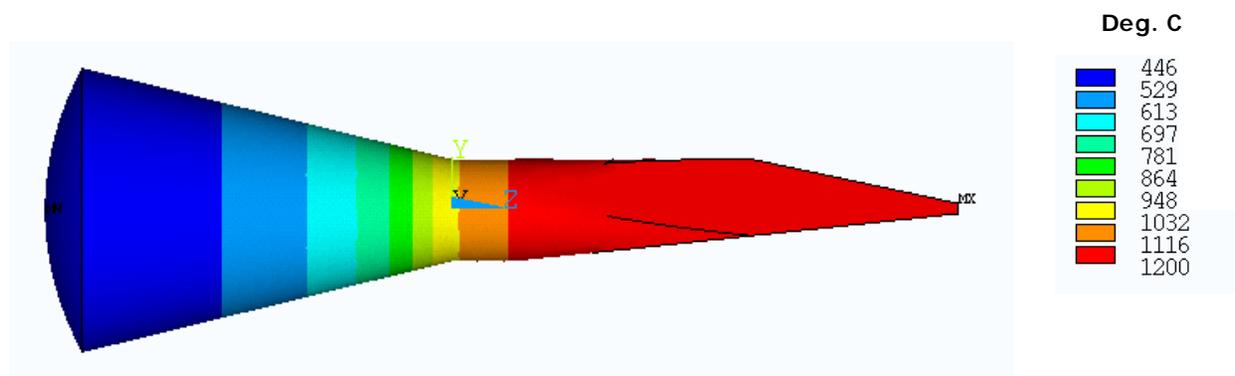
Figure 33.—Temperature distribution in sapphire crystal for covered cone design with a receiver temperature of 1200 °C.
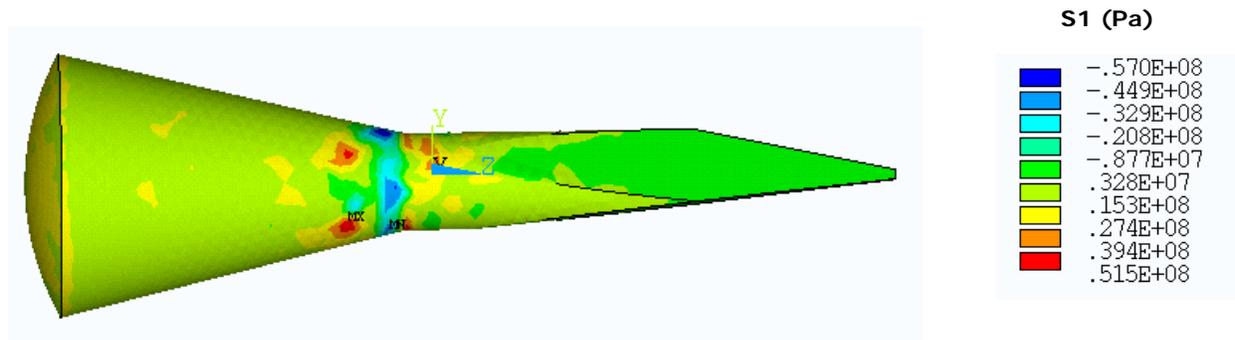
Figure 34.—First principal stress distribution in sapphire crystal for receiver temperature of 1200 °C with covered cone design. Stress results are in Pa.

Design of Future Solar Concentrators

Fracture in sapphire requires two ingredients: flaws and stresses. Both were present in the lenses. Twinning requires compression induced shear, with the magnitude depending on the surface finish and temperature. Intersecting twins can nucleate cracks, and thus twins must be designed against.

The stresses in the lenses are very low in magnitude. They are primarily thermal stresses due to differential expansions in the lens. Stresses could be generated either during the steady state operating condition of the lens at peak temperature or during transients such as during heat up. Although fractures

seemed to occur in both concentrators during their steady state run, the prospect of thermal stresses during a cool down must also be considered.

With the large preexisting flaws, the stresses in the lenses were sufficient to cause fracture. The plane of fracture in both was almost perfectly radial across the top curved lens surface. Beneath the top surface and into the cone body, fracture followed preferred crystal planes, but the radial cracking across the top of the lens that split the lenses into two primary halves (also along certain cleavage planes) strongly suggests that hoop stresses were the cause of fracture. The fracture origins were located near the rim of both lenses. Hence, one is led to the possibility that a temperature gradient may have existed across the face of the lens, such that the rim was cooler than the middle of the lens face. Such a temperature distribution would generate tensile hoop stresses near the rim. Various clamps and shields in place during the test sequence may have contributed to radial temperature gradients. The design of the shields and clamps should be reviewed prior to any future testing with the goal of minimizing radial temperature gradients.

The flaws (an impact crack in one case and a scratch in the other) were classic types commonly found in sapphire and most brittle materials for that matter. Sapphire is sensitive to chipping, scratches, and contact damage. The source of the two flaws that caused fracture of the concentrators appear to be handling damage incurred either during the preparation of the pieces, or afterwards during handling or installation in the test rig.

Sapphire is strong, hard, and scratch resistant if carefully prepared such as with bend bars and simple disks, but it is much harder to prepare complex parts without damage. Scratches, impacts and contact damage can weaken it considerably. Anything less than near-perfect preparation can lead to fracture if the part is exposed to any tensile stresses.

The two flaws were aberrant and were not ordinary grinding damage. Ordinary grinding damage and minor chipping were observed. Although they did not cause fracture in these two lenses, such flaws would be expected to play a role if the atypical impact and scratch damage had been prevented. Twins were noted in one lens, but they were incidental. Nevertheless, they could grow or new twins could nucleate with thermal cycling. They could generate strength limiting cracks and cause lens weakening.

The only ways to predict the survivability of future concentrators is to perform stress and reliability analyses or conduct costly proof testing. Multiple mechanisms of fracture exist in sapphire. The analyses will require data representing the expected failure modes for the use conditions. For elevated temperatures, compression along the c-axis results in the formation of r-plane twins at resolved shear stress as low as 12.6 MPa (Ref. 15). The r-plane twins nucleate cracks upon intersection (Refs. 15 and 16), and thus serve as a source of fracture. In addition, basal plane twinning has been observed beneath hardness indentations and abraded surface, and extensive basal plane twinning was generated from the compressive face of flexure beam (Ref. 7) at room temperature. For humid environments, stress corrosion produces slow crack growth in tensile regions (Refs. 17, 18, and 7). Slow crack growth has also been observed in c-axis fibers subjected to pure tension at elevated temperature (Ref. 19). Thermal shock loading has been noted to produce internal failure, although the specific mechanism was not identified (Ref. 20). In addition, slip can occur on the basal and prismatic plane at elevated temperatures. Generally this occurs at temperatures greater than 1000 °C and depends upon the strain rate (Refs. 21 to 23), however, under condition of confining pressure and compressive loading, basal slip at 600 °C and prismatic slip at temperatures low as 200 °C has been produced (Refs. 23 to 24). The shear stress levels for basal slip are on the order of 100 MPa or less for temperatures greater than 1100 °C and 300 MPa for prismatic slip (Ref. 25). The resolved shear stress for deformation of sapphire can be increased by doping with Cr^{3+} or Ti^{+4} ions (Ref. 26).

A review of the literature for this study revealed gaps in the data bases. For example, fracture branching distance constants are incomplete, and we had to make estimates of the appropriate branching constant. Fracture mirror constant tabulations for sapphire are also spotty. Additional fracture branching or fracture mirror data to fill the gaps would be very helpful and dramatically improve our ability to do post mortem failure analyses.

Any twinning, slip, or crack growth will likely cause aberrations in the light transmission within the RSC. Thus, for the temperature that the RSC is likely to encounter, the stress levels must be minimized,

and analyses for fast fracture, elevated temperature slow crack growth, and twinning should be performed. In order for such analyses to be valid, the input data must represent the condition and flaw population expected (i.e. similitude is required). Because handling damage is generally not well represented in input data, inspection and proof testing are frequently used for fracture critical hardware.

Conclusions

The first (exposed cone design) sapphire RSC fractured from a large contact crack associated with bruises on the lens surface that occurred during the grinding or polishing steps of the lens preparation. The estimated failure stresses were only 40 to 60 MPa and were consistent with a large crack being present at the fracture origin. Thus the component strength was well below values obtained with typical lab scale test coupons.

The second (covered cone design) sapphire RCS fractured from a large scratch and underlying precrack on the lens surface near the rim. The scratch was curved and rough, unlike nearby minor residual grinding damage, which was common. The estimated failure stress was on the order of 20 to 65 MPa and also was consistent with the presence of a large flaw at the origin.

Ideally, better handling and control of the parts would minimize the chances of the introduction of large flaws. Inspection protocols could be established to facilitate detection of such flaws, but it should be borne in mind that most of the flaw is beneath the surface. Surface traces of the flaw may be hard to detect or interpret.

Careful controls should be exercised during the machining and polishing or post machining treatment, such as etching or annealing, should be applied. Poor polishing, such as that observed, is referred to as a "short finish" and generally results in a very large variation in the measure strength. It must be realized that component strength and strength measured for ideal coupons can be very different unless very similar machining and handling is applied.

The stresses causing failure of the two RSCs resulted from thermal variation throughout the lens. One source of the thermal variation was the heat transfer characteristics of the component and its boundaries, however, other sources of potential thermal variation, such as the lens discoloration, need further investigation. Attention should be given to minimizing the radial temperature gradients on the front cured lens face. Due to the many issues discussed, creation of a reliable sapphire RSC will be difficult.

Recommendations

(1) Polishing with a specified procedure (Ref. 27) that eliminates subsurface damage (i.e., a "short finish"). This might be done only in critical areas in order to lower cost.

(2) Careful optical inspection of the component prior to testing to ensure that significant damage does not exist in critical areas.

(3) Elevated temperature annealing of the component to "heal" any unidentified machining damage. This is usually performed in air or flowing oxygen, and may be difficult because the component is so large that it may creep or brinnel under its own weight. Careful mounting of the component in the furnace will be required. An alternative to elevated temperature heat treatments is etching, similar in concept to that done on glass windows. However, this may require post-etching polishing.

(4) Improved thermal stress and reliability analyses to identify critical areas and quantify the component reliability. Further analyses will require knowledge of the failure mechanisms encountered in service. Ideally, analyses against fast fracture (via thermal stresses and shock), elevated temperature slow crack growth, and other internal mechanisms such as twinning should be considered. Unlike many ceramics, sapphire is sensitive to compressive stresses.

(5) Mechanical testing of coupons to generate strength, crack growth statistics, and fractographic constants for the use conditions. The strength of sapphire is a strong function of temperature, orientation,

surface finish, and stress state. Analysis of the concentrator should guide the coupon testing and the coupons must be prepared identically to the RSC for the test data to be representative and for any reliability analysis to be meaningful. Manufacturers generally can prepare flat coupons very well, however, curved surfaces are more difficult to prepare.

(6) Basic testing of coupons to determine the source of darkening and the affect on the transmission and heating characteristics of the sapphire.

(7) Analyze other single crystals such as SiC (Moissanite), which has become available in large diameters in recent years. As compared to sapphire, SiC exhibits some beneficial properties such as lower thermal expansion and higher thermal conductivity. It has similar fracture toughness (1.8 MPa√m). This material may therefore be very chip and contact damage sensitive. It also suffers from a low vapor pressure and active oxidation at low oxygen partial pressures. However, this might be mitigated by optical coatings.

References

1. X. Ning, R. Winston, J.O'Gallagher, "Dielectrically Totally reflecting Concentrator," Applied Optics, Vol. 26 (6), pp. 300–305, Optical Society of America, 1987.
2. D. Jenkins, R. Winston, J. Bliss, J. O'Gallagher, A Lewandowski, and C. Bingham, " Solar Concentration of 50,000 Achieved with Output Power Approaching 1 kW," J. Solar Energy Engineering, Vol. 118, pp. 141–145, 1996.
3. W.A. Wong and C.H. Castle, "High Temperature Solar Vacuum Testing of a Sapphire Refractive Secondary Concentrator," Proceedings of the Space Technology and Applications International Forum-STAIF 2002. American Institute of Physics Conference Proceedings, Vol. 608, 2002.
4. W.A. Wong, S.M. Geng, C.H. Castle, and R.P. Macosko, "Design, Fabrication and Test of a High Efficiency Refractive Secondary Concentrator for Solar Applications," Paper Number AIAA–2000–2998 from the Proceedings of the 35th Intersociety Energy Conversion Engineering Conference, 2000. Also NASA/TM—2000-210339.
5. George Rossman, Private communication, May 7, 2004, California Institute of Technology, Pasadena, CA.
6. N. Jacobson and R. Biering, "Materials Chemistry Issues in the Development of a Single-Crystal Solar/Thermal Refractive Secondary Concentrator," NASA/TM—2005-213625, 2005.
7. G.D. Quinn, "Fractography of Ceramics and Glasses," NIST Special Publication 960-16, National Institute of Standards and Technology, Gaithersburg, MD, 2007.
8. J.A. Salem, "Slow Crack Growth and Fracture Toughness of Sapphire for the International Space Station Fluids and Combustion Facility," NASA/TM—2006-214023, 2006.
9. J.J. Mecholsky, S.W. Freiman, and R.R. Rice, "Fractographic Analysis of ceramics," ASTM *Special Technical Publication 645*, B.M. Strauss and W.H. Cullen, eds., American Society for Testing and Materials, West Conshohocken, PA, pp. 336–379, 1977 .
10. R.W. Rice. "Ceramic Fracture Features, Observations, Mechanisms, and Uses," ASTM *Special Technical Publication 827*, J.J. Mecholsky and S.R. Powell, eds., American Society for Testing and Materials, West Conshohocken, PA, pp. 5–103,1982.
11. J.J. Mecholsky, and R.W. Rice, "Fractographic Analysis of Biaxial Failure in Ceramics," ASTM *Special Technical Publication 827*, J.J. Mecholsky and S.R. Powell, eds., American Society for Testing and Materials, West Conshohocken, PA, 185–193, 1982.
12. R.W. Rice, private communication, June 5, 2001.
13. J. B. Quinn, "Extrapolation of Fracture Mirror and Crack-Branch Sizes to Large Dimensions in Biaxial Strength Tests of Glass," *J. Am. Ceram. Soc.*, 82 [8] (1999) pp. 2126–2132.
14. J. Palko and S. Geng, Unpublished report on "Thermal and Structural Analysis of a Sapphire Refractive Secondary Concentrator Assembly," NASA Glenn research Center, Cleveland, OH, Mar. 2004.

15. W.D. Scott and K.K. Orr, "Rhombohedral Twinning in Alumina," *J. Am. Cerm. Soc.,* Vol. 66, pp. 27–32, 1983.
16. F. Schmid and D.C. Harris, "Effect of Crystal Orientation and Temperature on the Strength of Sapphire," *J. Am. Ceram. Soc.*, 81 [4], pp. 885–892, 1998.
17. T.A. Michalske, B.C. Bunker and S.W. Freiman, "Stress Corrosion of Ionic and Mixed Ionic/Covalent Solids, "*J. Am. Ceram. Soc.*, **69**, 10, pp. 721–724, 1986.
18. S.M. Wiederhorn, "Fracture of Ceramics," pp. 217–241 in National Bureau Special Publication 303, Proceedings of the conference on Mechanical and Thermal Properties of Ceramics, April 1–2, Gaithersburg, MD, 1968.
19. A. Sayir, "Time Dependent Strength of Sapphire Fibers at High Temperatures," in Advances in Ceramic Matrix Composites I, ed. N. Bansal, American Ceramic Society, pp. 691–702, 1993.
20. D. Zhu, N. Jacobson, and R Miller, "Thermal-Mechanical Stability of Single Crystal Refractive Concentrators for High-Temperature Solar Thermal Propulsion," proceedings of Renewable and Advanced Energy Systems for the 21st Century, April 11–15, Maui, HI, eds. R Hogan, Y. Kim, S Kleis, D. O'Neil and T. Tanaka, paper No. RAES99–7702, 1999.
21. J.B.J. Wacthman and L.H. Maxwell, "Plastic deformation of Ceramic-Oxide Crystals, II," *J. Am. Ceram. Soc.*, 40, 11, pp. 377–85, 1957.
22. M.L. Kronberg, "Dynamical Flow Properties of Single Crystals of Sapphire, I," *J. Am. Ceram. Soc.*, 45, 6, pp. 274–279, 1962.
23. H. Conrad, G. Stone, and K. Janowski, "Yielding and Flow of Sapphire in Tension and Compression," Trans. Met. Soc., AIME, 233, pp. 889–897, 1965.
24. J. Castaing, J. Cadoz, and S.H. Kirby, "Prismatic Slip of Al_2O_3 Single Crystals Below 1000 °C in Compression Under Hydrostatic Pressure," *J. Am. Ceram. Soc.*, 64, 9, pp. 504–511, 1981.
25. D.J. Gooch and G.W. Grooves, "Prismatic Slip on Sapphire," *J. Am. Ceram. Soc.*, 55, 2, pp. 105, 1972.
26. B.J. Pletka, A.H. Heuer, and T.E. Mitchell, "Work-Hardening in Sapphire," Acta Metall., 25, pp. 25–33, 1977.
27. J.A. Salem, "Handbook for Recommended Material Removal Processes for Advanced Ceramic Test Specimens and Components," NASA–HDBK–6007, Nov. 2007.

Appendix A.—Examination Techniques for Twins

Sapphire sometimes forms twins in response to thermomechanical loading. They may be harmless or they can cause fracture, particularly if intersecting twins nucleate cracks. Twinning will likely cause aberrations in the light transmission within the RSC and conceivable it could create hot spots. Twins can be very small and difficult to detect or very large and easy to detect. Large and small twins were detected in the concentrators. Twins can be distinguished from fracture surfaces since twins are extremely flat and straight, whereas most fracture surfaces have some irregularities. The simplest examination procedure is to position the component in a Polariscope as shown in Figure A1, and rotate the component around with different orientations. An improvised Polariscope that is in some respects easier to use is shown in Figure A2.


(a)

(b)

Figure A1.—Classic style Polariscope. (a) The component is placed between the polarizer eyepieces and the illuminated polarizing screen. (b) is a picture of piece 1 of concentrator 1. The photo was taken by a digital camera focused through one eyepiece. The very large twin appears as a light colored band running diagonally through the piece (white arrows). It is not a fracture plane.

(a)
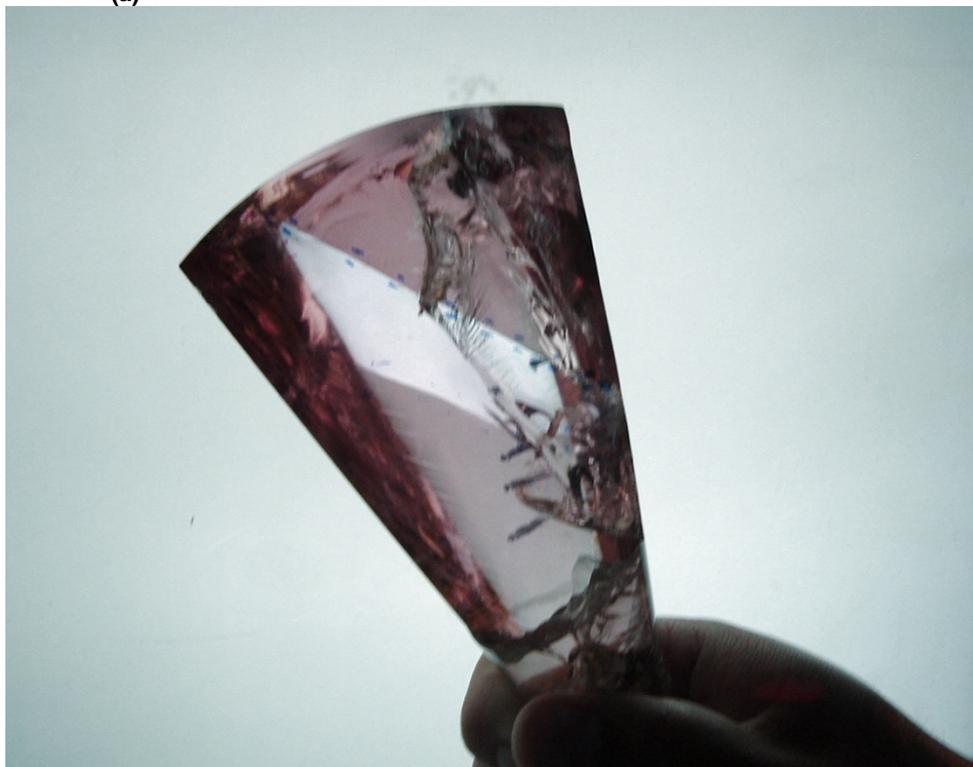
(b)

Figure A2.—An improvised Polariscope examination device. (a) shows a common light box is with two polymer polarizing sheets. One is clipped to the light box, the other is held by a clamp on the post in the foreground. Piece 1 of concentrator 1 is placed in between and rotated about. (b) shows a photo of the twin.

A third way to look for twins is to use conventional reflected or transmitted illumination and look for reflections or slight refractions of the light. Figure A3 shows the set up used to find additional twins in concentrator 1.
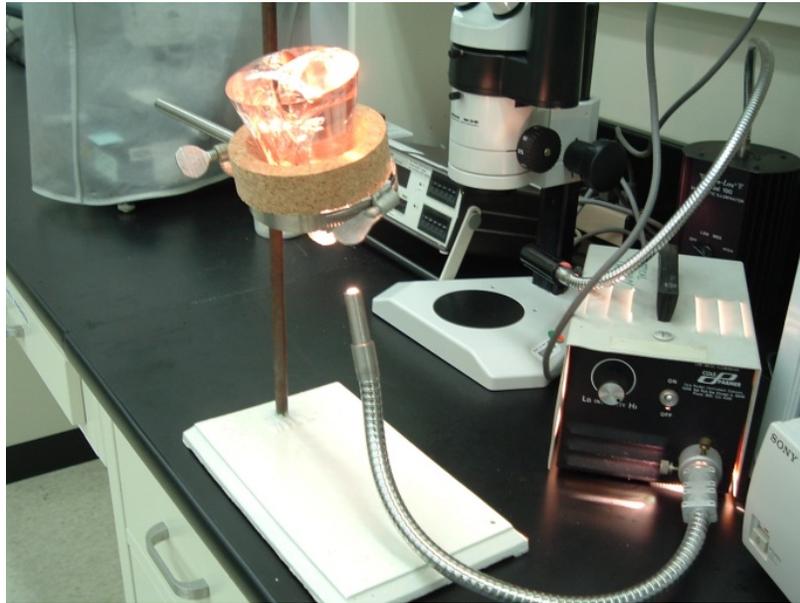

(a)
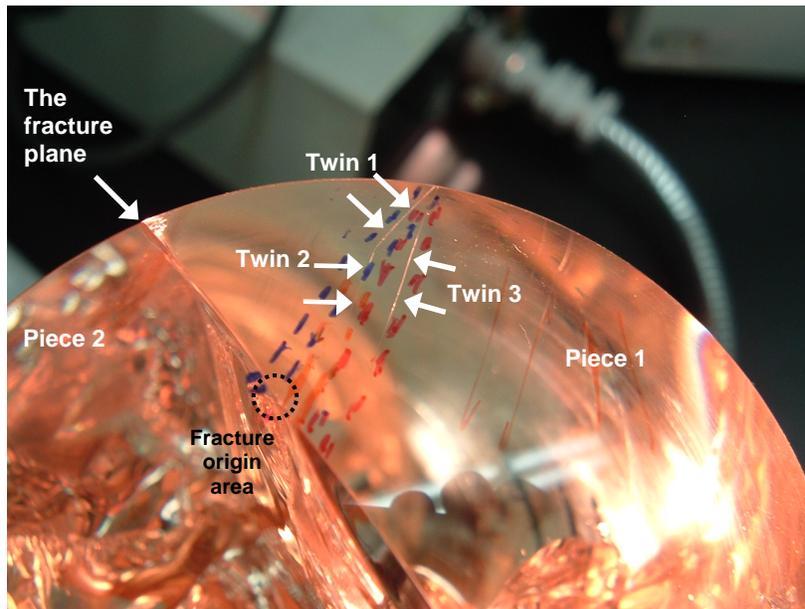
(b)

Figure A3.—Transmitted illumination was used to detect small twins. (a) shows the two pieces of concentrator 1 mounted in a soft cork ring on a common ring stand. A fiber optic light source was directed up through the body. (b) shows a digital camera photograph of the front face of RSC no. 1. Color felt tip dashed marker lines were marked on the surface to bracket two twins, which are the very thin white lines marked by the white arrows. (c) shows other twins on the same surface. The lighting and component orientation has to be changed to accentuate each twin set since it is difficult to get all twins visible at the same time. Twins 5a and b are tiny short segments. Twin 4 is longer.

(c)
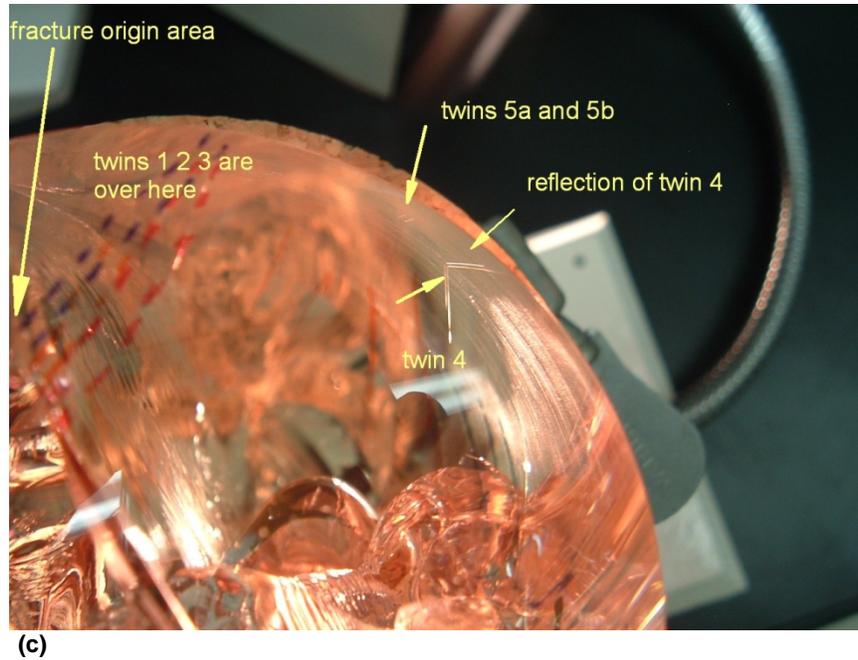
Figure A3.—(Concluded.) Transmitted illumination was used to detect small twins. (a) shows the two pieces of concentrator 1 mounted in a soft cork ring on a common ring stand. A fiber optic light source was directed up through the body. (b) shows a digital camera photograph of the front face of RSC no. 1. Color felt tip dashed marker lines were marked on the surface to bracket two twins, which are the very thin white lines marked by the white arrows. (c) shows other twins on the same surface. The lighting and component orientation has to be changed to accentuate each twin set since it is difficult to get all twins visible at the same time. Twins 5a and b are tiny short segments. Twin 4 is longer.

1. REPORT DATE *(DD-MM-YYYY)* 01-12-2009	2. REPORT TYPE Technical Memorandum	3. DATES COVERED *(From - To)*

4. TITLE AND SUBTITLE Failure Analysis of Sapphire Refractive Secondary Concentrators	5a. CONTRACT NUMBER
	5b. GRANT NUMBER
	5c. PROGRAM ELEMENT NUMBER
6. AUTHOR(S) Salem, Jonathan, A.; Quinn, George, D.	5d. PROJECT NUMBER
	5e. TASK NUMBER
	5f. WORK UNIT NUMBER WBS 984754.02.07.03.16.03

7. PERFORMING ORGANIZATION NAME(S) AND ADDRESS(ES) National Aeronautics and Space Administration John H. Glenn Research Center at Lewis Field Cleveland, Ohio 44135-3191	8. PERFORMING ORGANIZATION REPORT NUMBER E-17063

9. SPONSORING/MONITORING AGENCY NAME(S) AND ADDRESS(ES) National Aeronautics and Space Administration Washington, DC 20546-0001	10. SPONSORING/MONITOR'S ACRONYM(S) NASA
	11. SPONSORING/MONITORING REPORT NUMBER NASA/TM-2009-215802

12. DISTRIBUTION/AVAILABILITY STATEMENT
Unclassified-Unlimited
Subject Categories: 27 and 20
Available electronically at http://gltrs.grc.nasa.gov
This publication is available from the NASA Center for AeroSpace Information, 443-757-5802

13. SUPPLEMENTARY NOTES

14. ABSTRACT
Failure analysis was performed on two sapphire, refractive secondary concentrators (RSC) that failed during elevated temperature testing. Both concentrators failed from machining/handling damage on the lens face. The first concentrator, which failed during testing to 1300 °C, exhibited a large *r*-plane twin extending from the lens through much of the cone. The second concentrator, which was an attempt to reduce temperature gradients and failed during testing to 649 °C, exhibited a few small twins on the lens face. The twins were not located at the origin, but represent another mode of failure that needs to be considered in the design of sapphire components. In order to estimate the fracture stress from fractographic evidence, branching constants were measured on sapphire strength specimens. The fractographic analysis indicated radial tensile stresses of 44 to 65 MPa on the lens faces near the origins. Finite element analysis indicated similar stresses for the first RSC, but lower stresses for the second RSC. Better machining and handling might have prevented the fractures, however, temperature gradients and resultant thermal stresses need to be reduced to prevent twinning.

15. SUBJECT TERMS
Sapphire; Thermal stresses; Solar energy; Space exploration; Polishing; Strength; Fractures; Failure analysis; Twinning; Concentrator

16. SECURITY CLASSIFICATION OF:			17. LIMITATION OF ABSTRACT	18. NUMBER OF PAGES	19a. NAME OF RESPONSIBLE PERSON STI Help Desk (email:help@sti.nasa.gov)
a. REPORT U	b. ABSTRACT U	c. THIS PAGE U	UU	44	19b. TELEPHONE NUMBER *(include area code)* 443-757-5802

Standard Form 298 (Rev. 8-98)
Prescribed by ANSI Std. Z39-18